Received: 18 June 2019 | Revised: 10 October 2019 | Accepted: 11 October 2019

DOI: 10.1111/bre.12416

ORIGINAL ARTICLE

Basin Research | IAS EAGE | WILEY

Axial and transverse deep-water sediment supply to syn-rift fault terraces: Insights from the West Xylokastro Fault Block, Gulf of Corinth, Greece

Timothy M. Cullen[1,2] | **Richard E. Ll. Collier**[1] | **Robert L. Gawthorpe**[2] | **David M. Hodgson**[1] | **Bonita J. Barrett**[1]

[1]School of Earth and Environment, University of Leeds, Leeds, United Kingdom

[2]Department of Earth Sciences, University of Bergen, Bergen, Norway

Correspondence
Timothy M. Cullen, School of Earth and Environment, University of Leeds, Leeds, United Kingdom.
Email: t.m.cullen1@leeds.ac.uk

Funding information
Research Council of Norway, Grant/Award Number: 255229/E30; ConocoPhillips; DNO; Equinor; Tullow Oil; Neptune; Aker BP University of Leeds. TMC and RLG also acknowledge VISTA for funding to a visiting scholarship (TMC) and VISTA professorship (RLG) at the University of Bergen

Abstract

Deep-water syn-rift systems develop in partially- or transiently-linked depocentres to form complicated depositional architectures, which are characterised by short transport distances, coarse grain sizes and a wide range of sedimentary processes. Exhumed systems that can help to constrain the tectono-stratigraphic evolution of such systems are rare or complicated by inversion tectonics. Here, we document a mid-Pleistocene deep-water syn-rift system fed by Gilbert-type fan deltas in the hangingwall of a rift margin fault bounding the West Xylokastro Horst block, on the southern margin of the Gulf of Corinth, Greece. Structural and stratigraphic mapping combined with digital outcrop models permit observations along this syn-rift depositional system from hinterland source to deep-water sink. The West Xylokastro Fault hangingwall is filled by two distinct sediment systems; an axial system fed by coarse-grained sediment gravity flows derived from fault-tip Gilbert-type fan deltas and a lateral system dominated by mass transport deposits fed from an evolving fault-scarp apron. Abrupt changes in stratigraphic architecture across the axial system are interpreted to record changes in relative base level, sediment supply and tectonics. Locally, depositional topography and intra-basinal structures controlled sediment dispersal patterns, from bed-scale infilling of local rugose topography above mass transport complexes, to basin-scale confinement from the fault scarp apron. These acted to generate a temporally and spatially variable, heterogeneous stratigraphic architecture throughout the basin-fill. The transition of the locus of sedimentation from a rift margin to a fault terrace through the syn-sedimentary growth of a basinward fault produced regressive surfaces updip, which manifest themselves as channels in the deep-water realm and acted to prograde the system. We present a new conceptual model that recognises coeval axial and transverse systems based on the stratigraphic architecture around the West Xylokastro fault block that emphasizes the lateral and vertical heterogeneity of rift basin-fills with multiple entry points.

KEYWORDS

deep-water fan, Gilbert deltas, Gulf of Corinth, rift basins, sand fairway, sediment routing, structural highs, syn-rift, Xylokastro

1 | INTRODUCTION

The depositional architecture of deep-water syn-rift systems can record the interaction of axial (fault parallel) and transverse (fault perpendicular) sediment supply systems, fault-related topography and short-scale spatial changes in basin physiography. However, existing models for multi-input deep-water syn-rift systems lack details on the nature and controls of stratigraphic architecture (Fraser et al., 2003; Fugelli & Olsen, 2007; Strachan et al., 2013). Outcrop studies are vital for understanding the evolution of these variable and localised depocentres (e.g. Barrett et al., 2019; Gawthorpe, Fraser, & Collier, 1994; Gawthorpe et al., 2018; Henstra et al., 2016; Rohais, Eschard, Ford, Guillocheau, & Moretti, 2007; Rohais, Joannin, et al., 2007; Sharp, Gawthorpe, Underhill, & Gupta, 2000; Strachan et al., 2013). Distinguishing the distribution and interplay of different input systems is challenging, particularly in cases where the hinterland provenance is similar. Exhumed systems can provide information in the scale gap between core and seismic observations of such systems. However, exhumed systems are comparatively rare; meaning the variability of stratigraphic architecture at the mesoscale (10s to 100s of metres) is seldom captured in stratigraphic models.

Many deep-water syn-rift systems have been studied using subsurface datasets, including the Brae trend of the South Viking Graben (Fraser et al., 2003; Turner & Allen, 1991; Turner, Bastidas, Connell, & Petrik, 2018; Turner, Cronin, et al., 2018), and the East African Rift (Scholz et al., 1998; Scholz, Rosendahl, & Scott, 1990; Soreghan, Scholz, & Wells, 1999). They are characterized by small, isolated to partially-linked, depocentres with narrow or entirely absent shelves or littoral zones, and high sediment supply, which in deep-water systems leads to a wide range of gravity current processes. Footwall sourced, Hangingwall aprons, dominated by rock-fall deposits from fault scarp degradation, form a principal endmember (Bilal, McClay, & Scarselli, 2018; Gawthorpe & Leeder, 2000; Reading & Richards, 1994; Sharp et al., 2000). Footwall-sourced systems are well-documented with conceptual models developed from numerous subsurface and outcrop studies, for example, Oseberg systems (Ravnås & Steel, 1997), the 'Brae Play' trend of the South Viking Graben (Garland, Haughton, King, & Moulds, 1999; Jones, Cronin, & Allerton, 2018; Turner & Allen, 1991; Turner, Bastidas, et al., 2018; Turner, Cronin, et al., 2018), and the Wollaston Ford Grp., Greenland (Henstra et al., 2016). Spatially distinct but coeval input systems will respond to the same allogenic controls but different autogenic controls. However, axial and mixed syn-rift deep-water fan styles are comparatively less studied, for example, Lower Kimmeridge of the Strathspey-Brent systems (McLeod, Underhill, Davies, & Dawers, 2002) or Kimmeridgian systems in the region of the J-Ridge in the Central North Sea (McArthur, Hartley, Archer, Jolley, & Lawrence, 2016). Most Exhumed deep-water syn-rift systems exhibit one main input system (e.g. Gulf of Suez – Gupta, Underhill, Sharp, & Gawthorpe, 1999; Leppard & Gawthorpe, 2006; Strachan et al., 2013), and systems where axial and transverse systems coexisted, so that the balance of allogenic and autogenic controls can be understood, have not been documented.

Highlights

- Outcrop example of a deepwater syn-rift clastic system which can be linked from source to sink
- Integration of field observations and digital outcrop models provides mesoscale (10s-100s m) characterization of stratigraphic architecture of axial and transverse deepwater syn-rift depositional systems
- Mass-transport dominated, transverse aprons can impart control on axial, delta-derived systems
- Variable basin floor topography from intra-basinal faults, mass-transport deposits and interacting systems produce substantial vertical and lateral heterogeneity within axial systems
- New conceptual models for the evolution and distribution of deepwater, coarse-grained depositional systems within syn-rift settings

Here, we summarize stratigraphic mapping and mesoscale architectural observations within the West Xylokastro Fault Block (WXFB), Gulf of Corinth, Greece, to develop a new conceptual model for deep-water syn-rift depositional systems fed by coeval transverse and axially input systems. The syn-rift infill of the WXFB was principally fed by the Evrostini and Ilias Gilbert-type deltas at the western tip of a structural high, the Xylokastro Horst (Figures 1 and 2) (Gobo, Ghinassi, & Nemec, 2014, 2015; Gobo, Ghinassi, Nemec, & Sjursen, 2014; Rohais, Eschard, et al., 2007; Rohais, Joannin, et al., 2007; Rohais, Eschard, & Guillocheau, 2008; Rubi, Rohais, Bourquin, Moretti, & Desaubliaux, 2018; Zhong, Escalona, Sverdrup, & Bukta, 2018). The related deep-water sediments, the Rethi-Dendro Formation, are exposed ~10 km basinward from these fan deltas (Gawthorpe et al., 2018; Koutsouveli, Mettos, Tsapralis, Tsala-Monopoli, & Iokim, 1989; Leeder et al., 2012; Tsoflias, Fleury, & Iokim, 1993). The exceptional exposures of the WXFB permit outcrop-scale links from hinterland source to deep-water sink within a syn-rift basin. This study aims to integrate the structural and stratigraphic evolution of the WXFB to address the following research questions:

a. What are the characteristics of deep-water syn-rift deposits connected to sedimentary inputs such as Gilbert-type fan deltas?

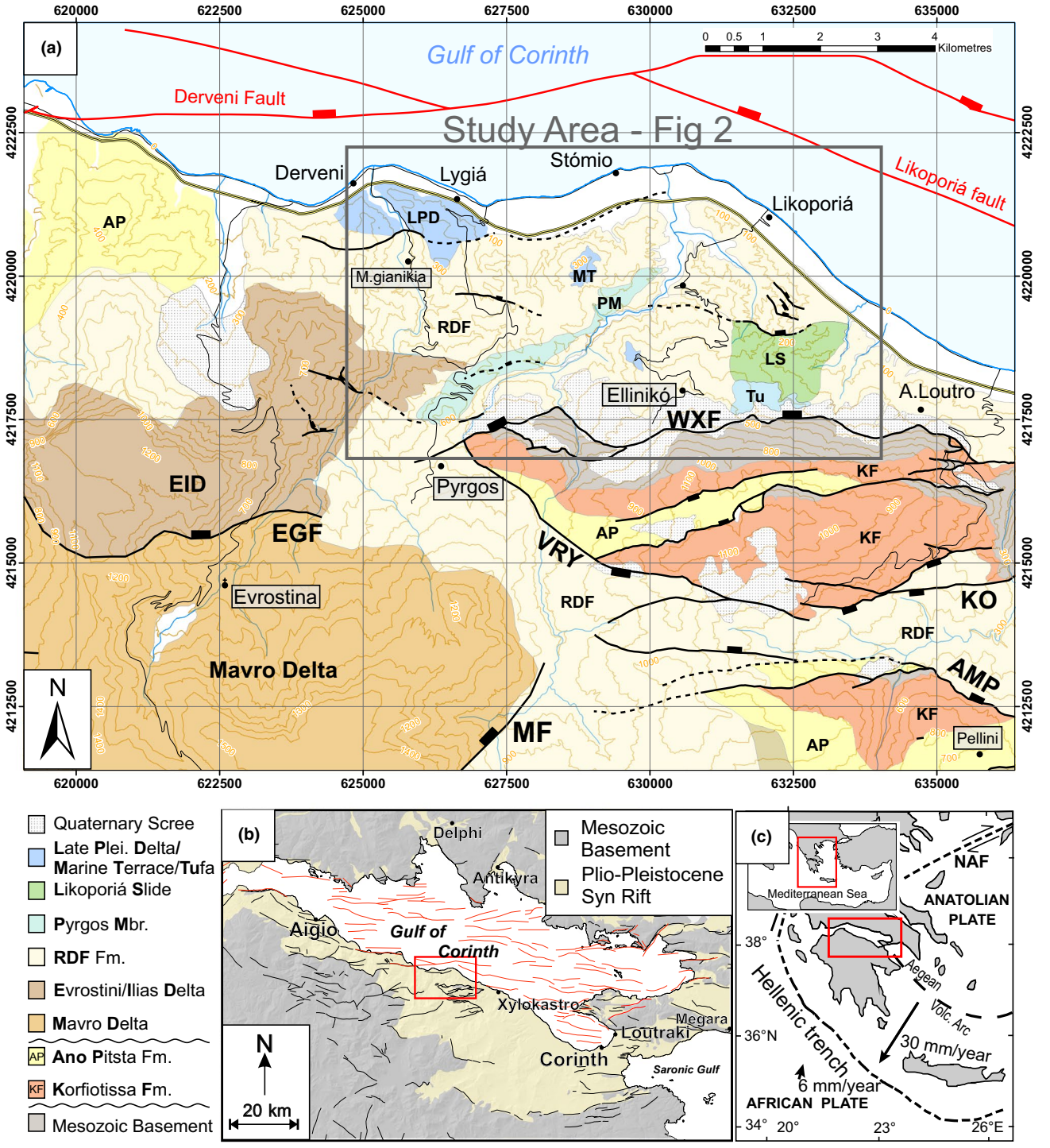

FIGURE 1 Location overview for the study area within the Gulf of Corinth. (a) Geological map for the study area on the southern, central margin of the Gulf of Corinth. Bold letters in the key correlate to labelled units on the map. WXF – West Xylokastro Fault, VRY – Vryssoules Fault, KO – Koutsos Fault, AMP – Amphithea Fault, MF – Mavro Fault, EGF – Evrostini Growth Fault. Red faults are currently active. Grey box highlights the mapping area within this study. Coordinates are UTM (in metres) for zone 34N. (b) Gulf of Corinth geological map highlighting the distribution of Pre-Rift and Syn-Rift stratigraphy and the location of the area within central Greece. All mapping were constructed and modified from Gawthorpe et al. (2018), compiled from Ford et al. (2013), Ford et al. (2016), Nixon et al. (2016), Skourtsos unpb. and author's own mapping. Red box indicates the locale focused on in this paper

b. How do axially fed deep-water fairways interact with transverse systems?
c. How can conceptual stratigraphic models capture multi-input syn-rift systems?

2 | GEOLOGICAL SETTING

The Gulf of Corinth is an active rift that initiated ~5 Ma in the very latest Miocene or early Pliocene (Beckers et al., 2015; Bell et al., 2009; Briole et al., 2000; Collier & Dart, 1991; Doutsos & Piper, 1990; Doutsos & Poulimenos, 1992; Gawthorpe et al., 2018; Goldsworthy & Jackson, 2001; Hemelsdaël & Ford, 2016; McNeil et al., 2005; Pirazzoli, Stiros, Fontugne, & Arnold, 2004; Rohais, Eschard, et al., 2007; Rohais & Moretti, 2017; Skourtsos & Kranis, 2009; Taylor et al., 2011). The rift forms in response to regional NE-SW back-arc extension associated with subduction of the African Plate under the European and Anatolian plates (Armijo, Meyer, King, Rigo, & Papanastassiou, 1996; Westaway, 2002). The rift overlies the Pindos thrust sheet, a ~1.3 km thick succession of Mesozoic carbonates and Cenozoic flysch arranged in N-S striking thrust domains, oblique to the NW-SE to E-W rift fabric (Ford et al., 2013; Gawthorpe et al., 2018; Rohais & Moretti, 2017; Skourtsos & Kranis, 2009; Skourtsos, Kranis, Zambetakis-Lekkas, Gawthorpe, & Leeder, 2016). A distributed fault network developed a set of depocentres filled with alluvial and fluvial depositional systems during an early rift phase probably lasting from 5 to ~3 Ma, which ultimately developed into a central 'Lake Corinth' (Ford, Hemelsdaël, Mancini, & Palyvos, 2016; Ford et al., 2013; Gawthorpe et al., 2018; Nixon et al., 2016; Rohais, Eschard, et al., 2007; Rohais, Joannin, et al., 2007).

The onshore deep-water stratigraphy of the central Gulf of Corinth comprises the Rethi-Dendro Formation, which was initially deposited in Lake Corinth during the late 'Rift 1' and 'Rift 2' phases, between ~2–2.5 and ~0.5–0.7 Ma (Gawthorpe et al., 2018; Leeder et al., 2012; Figure 2b). Numerous fan deltas sourced from the Olvios drainage catchment feed the Rethi-Dendro Formation (Fernández-Blanco, Gelder, Gallen, Lacassin, & Armijo, 2019; Gawthorpe et al., 2018; de Gelder et al., 2019). These fan deltas (Kyllini, Mavro, Evrostini/Ilias) migrated northward in response to progressive basin deepening events and narrowing of the rift (de Gelder et al., 2019; Gawthorpe et al., 2018). Migration of fault activity between Rift 1 and Rift 2 to a co-linear, E-W trending rift margin in the position of the West Xylokastro Fault favoured the development of the giant Evrostini and Ilias Gilbert-type fan deltas (Figure 1; Ford et al., 2016; Gawthorpe et al., 2018; Rohais et al., 2008). These prograded into 300–600 m of water and fed downdip deep-water systems in the WXFB depocentre (Ford et al., 2016; Gawthorpe et al., 2018; Gobo, Ghinassi, & Nemec, 2014; Gobo et al., 2015; Rohais, Eschard, et al., 2007; Rohais, Joannin, et al., 2007; Rubi et al., 2018; Zhong et al., 2018). The Evrostini/Ilias fan delta system was active for much of the Mid-Pleistocene prior to another northward migration of the shoreline and a drainage reversal in the Late-Pleistocene (de Gelder et al., 2019; Fernández-Blanco et al., 2019; Gawthorpe et al., 2018; Rohais, Eschard, et al., 2007; Rohais, Joannin, et al., 2007). The growth of the basinward Likoporiá and Derveni Faults (Figure 1) occurred ~750 ka (de Gelder et al., 2019; Fernández-Blanco et al., 2019; Gawthorpe et al., 2018; Nixon et al., 2016) and are now incised by the antecedent Dervenios River. The presently active Likoporiá and Derveni faults control the modern coastline, and their footwall uplift has exhumed the WXFB. Offshore stratigraphy is split into two key units (Nixon et al., 2016); the lowermost (SU1 from ~2–1.5 Ma to 0.6 Ma) may be the offshore equivalent to the Rethi-Dendro observed onshore (Gawthorpe et al., 2018; McNeil et al., 2019; Nixon et al., 2016).

3 | METHODOLOGY

Stratigraphic and structural mapping in the WXFB has permitted description of stratigraphy across a 40 km^2 area downdip of the Evrostini and Ilias fan deltas, which has to date remained undifferentiated (Figures 1 and 2). In the absence of confident biostratigraphic or chronostratigraphic markers, correlations rely on dip-projection of observable stratigraphic surfaces or extensive intervals (i.e. pervasive fine-grained intervals). This approach is achieved through the construction of cross-sections, structural contouring and photogrammetry. Photogrammetric models, using photographs collected from a DJI Phantom 3 Professional and DJI Mavic Pro UAV, were built in Agisoft Photoscan and interpreted in LIME. These models (shown in the Supplementary Information) permit investigation in inaccessible areas to support stratigraphic

FIGURE 2 (a) Detailed geological map generated in this study. MT = Marine Terrace, WXF = WXF, VRY = Vryssoules Fault. Cross section (Figure 3) localities are provided in dark blue dots, with other figures in this paper referenced by white outlook points. Stratigraphic key for the map shows colours and relative ages of mapped units. (b) Simplified chronostratigraphy for the studied section (grey box) modified from Gawthorpe et al. (2018) and put in comparison with other stratigraphic schemes for the area (Nixon et al., 2016; Rohais et al., 2008). AF = Amphithea Fault, KF = Kyllini Fault, MF = Mavro Fault, WXF = WXF, LF = Likoporiá Fault, K = Kyllini, *M* = Mavro, E/I = Evrostini/Ilias

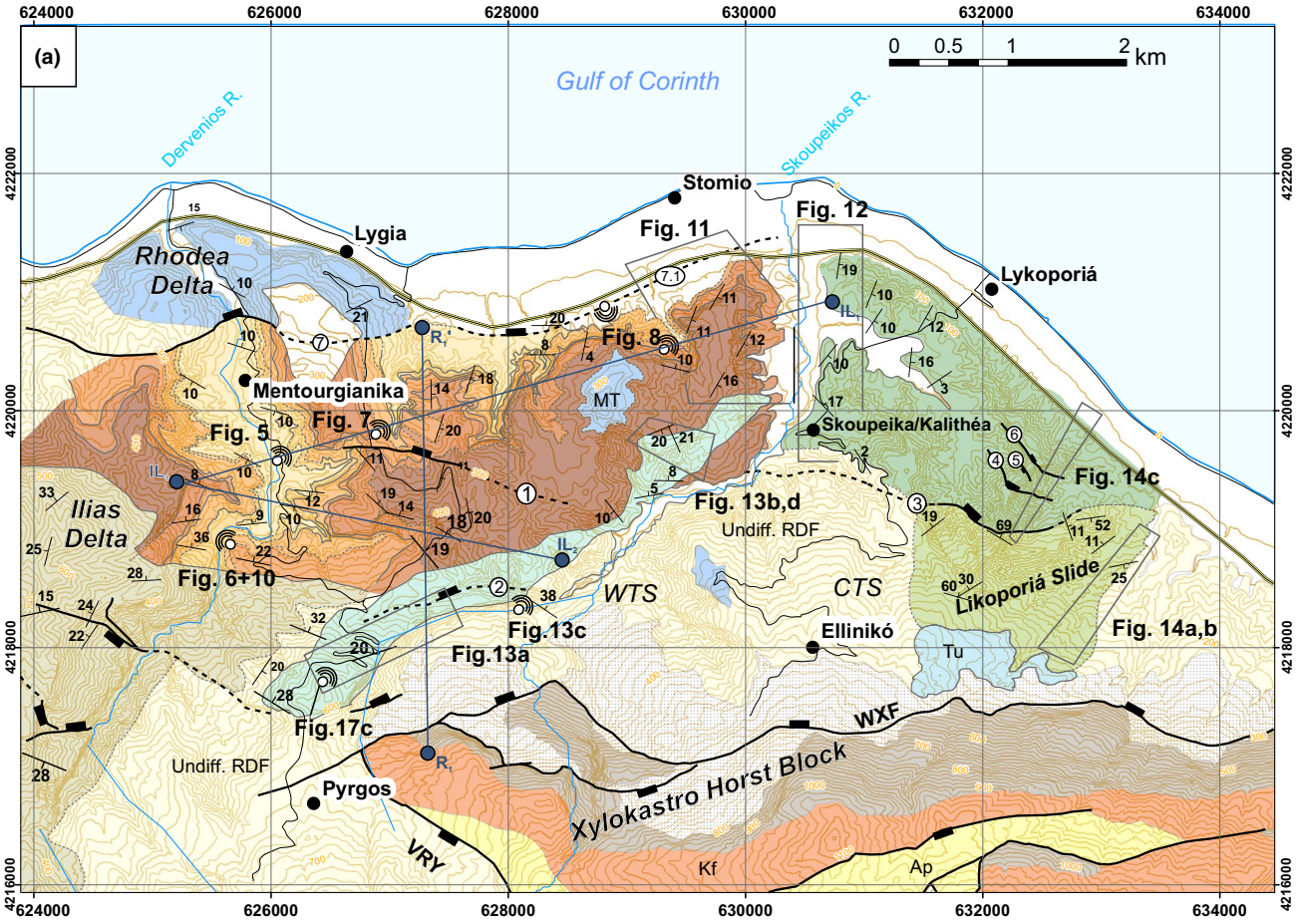
(a)
Gulf of Corinth
Dervenios R.
Skoupeikos R.
0 0.5 1 2 km
Stomio
Lygia
Rhodea Delta
Fig. 11
Fig. 12
Lykoporiá
Fig. 8
Mentourgianika
MT
Fig. 5
Fig. 7
Skoupeika/Kalithéa
Fig. 14c
Ilias Delta
Fig. 13b,d
Undiff. RDF
Fig. 6+10
WTS
CTS
Likoporiá Slide
Fig. 13c
Fig.13a
Elliniko
Tu
Fig. 14a,b
Fig.17c
WXF
Undiff. RDF
Pyrgos
Xylokastro Horst Block
VRY
Kf
Ap
624000
626000
628000
630000
632000
634000
4222000
4220000
4218000
4216000

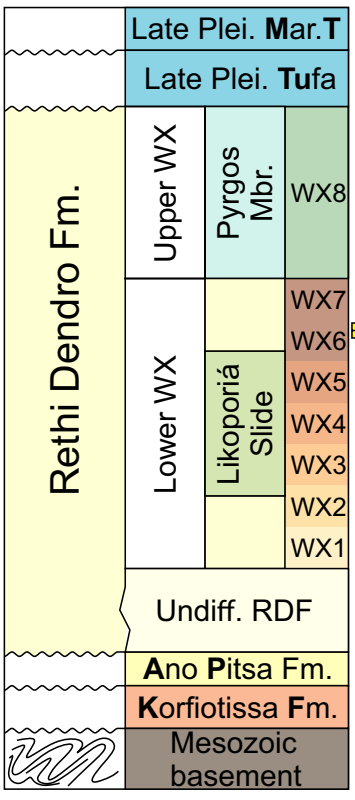
Rethi Dendro Fm.
Late Plei. Mar.T
Late Plei. Tufa
Upper WX
Pyrgos Mbr.
WX8
Lower WX
Likoporiá Slide
WX7
WX6
WX5
WX4
WX3
WX2
WX1
Undiff. RDF
Ano Pitsa Fm.
Korfiotissa Fm.
Mesozoic basement

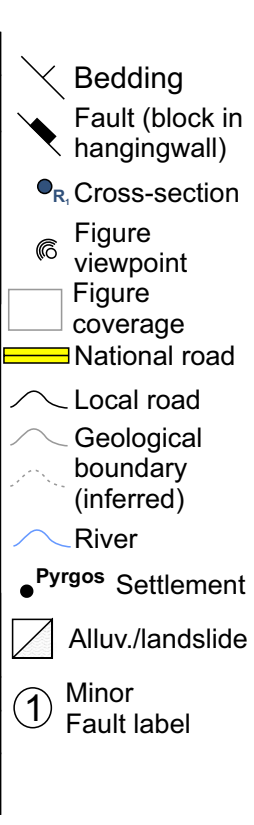
Bedding
Fault (block in hangingwall)
Cross-section
Figure viewpoint
Figure coverage
National road
Local road
Geological boundary (inferred)
River
Pyrgos Settlement
Alluv./landslide
Minor Fault label

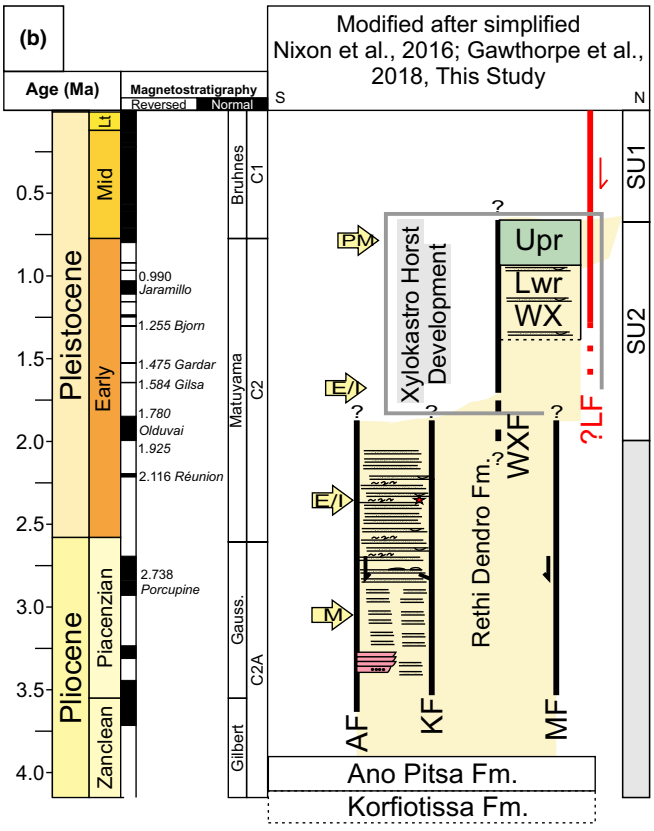
(b)
Age (Ma)
Magnetostratigraphy
Reversed
Normal
Pleistocene
Pliocene
Early
Mid
Lt
Piacenzian
Zanclean
0.990 Jaramillo
1.255 Bjorn
1.475 Gardar
1.584 Gilsa
1.780 Olduvai
1.925
2.116 Réunion
2.738 Porcupine
Bruhnes C1
Matuyama C2
Gauss. C2A
Gilbert
Modified after simplified Nixon et al., 2016; Gawthorpe et al., 2018, This Study
S
N
SU1
SU2
PM
E/I
M
Xylokastro Horst Development
Upr
Lwr
WX
WXF
?LF
Rethi Dendro Fm.
AF
KF
MF
Ano Pitsa Fm.
Korfiotissa Fm.

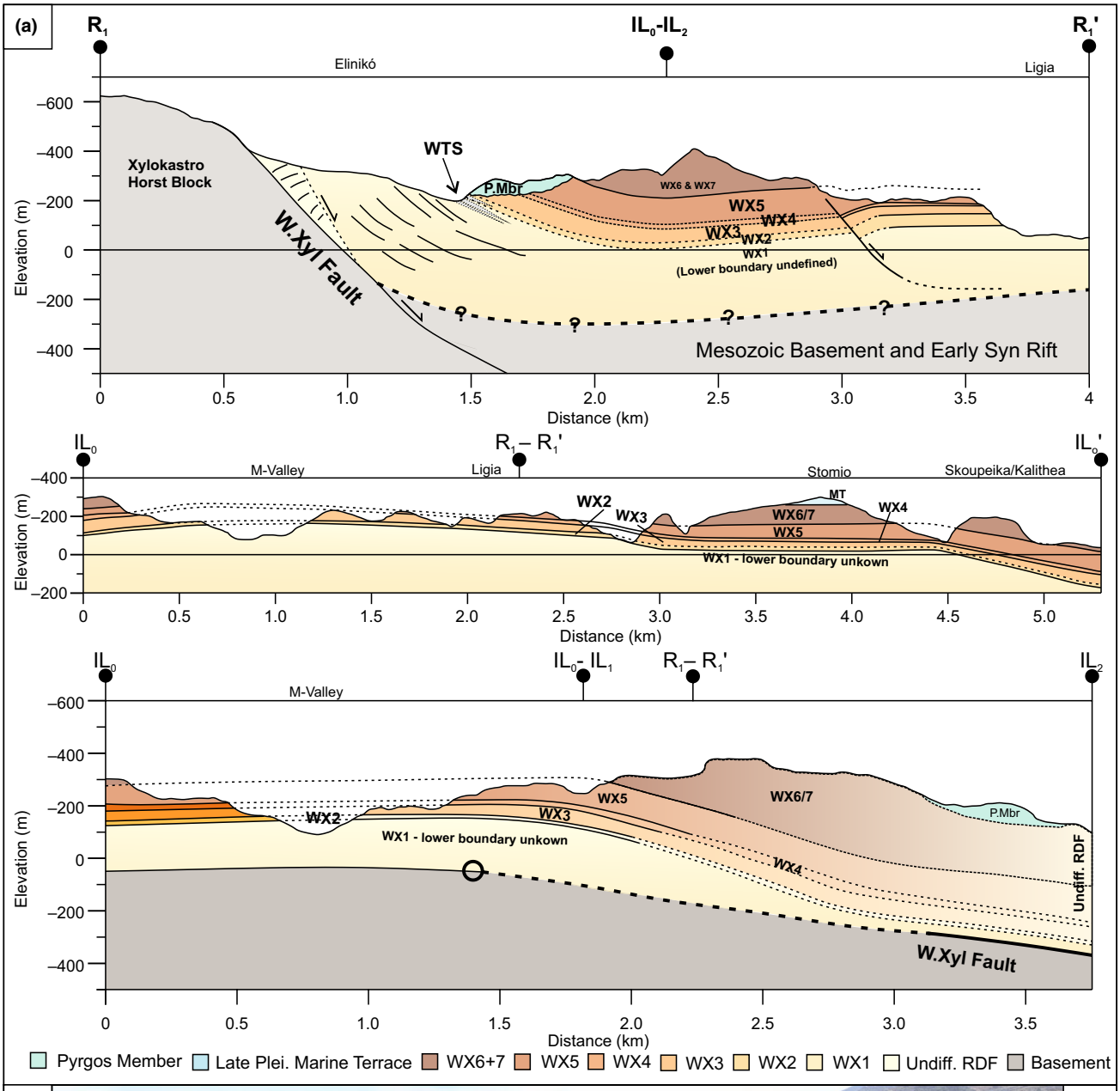
(a)
R1
IL0-IL2
R1'
Elinikó
Ligia
Xylokastro Horst Block
WTS
P.Mbr
WX6 & WX7
WX5
WX4
WX3
WX2
WX1
(Lower boundary undefined)
W.Xyl Fault
Mesozoic Basement and Early Syn Rift
Elevation (m)
Distance (km)
IL0
R1 – R1'
IL0'
M-Valley
Ligia
Stomio
Skoupeika/Kalithea
MT
WX6/7
WX1 - lower boundary unkown
IL0
IL0- IL1
R1 – R1'
IL2
M-Valley
WX2
WX3
WX5
WX6/7
P.Mbr
WX1 - lower boundary unkown
WX4
Undiff. RDF
W.Xyl Fault
Pyrgos Member
Late Plei. Marine Terrace
WX6+7
WX5
WX4
WX3
WX2
WX1
Undiff. RDF
Basement

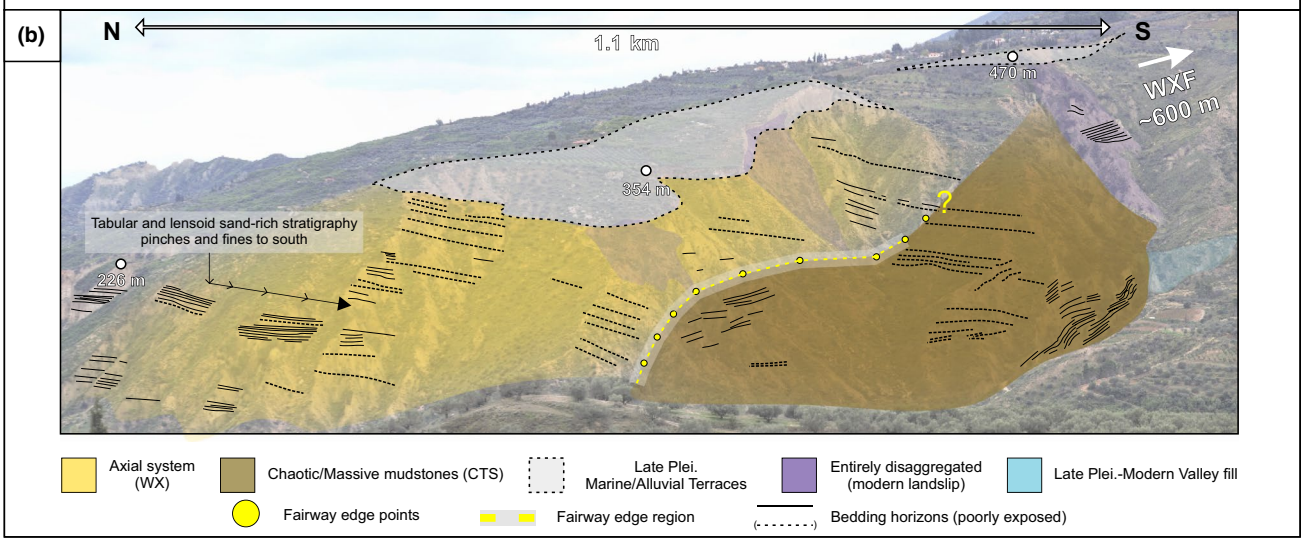
(b)
N
1.1 km
S
470 m
WXF
~600 m
354 m
Tabular and lensoid sand-rich stratigraphy pinches and fines to south
226 m
Axial system (WX)
Chaotic/Massive mudstones (CTS)
Late Plei. Marine/Alluvial Terraces
Entirely disaggregated (modern landslip)
Late Plei.-Modern Valley fill
Fairway edge points
Fairway edge region
Bedding horizons (poorly exposed)

FIGURE 3 (a) Simplified cross-sections for the areas showing the general structural arrangement of stratigraphy. The basal RDF/WX to Pre-rift boundary is not seen in the area. (b) Annotated photo panel of patchy exposures to the south of Kalithea/Skoupeikia highlighting the relationship between the axial undifferentiated RDF system and the chaotic mudstones of the Central Transverse System

correlations and collect structural (i.e. bedding dip) and stratigraphic (i.e. thickness) data. These units are described by their bounding surfaces and depositional elements. A detailed sedimentological process study is beyond the scope of this paper and as such, we describe the stratigraphy in terms of depositional elements (Section 4.2) to inform interpretations of the larger scale evolution of the WXFB.

4 | STRUCTURE AND STRATIGRAPHY

4.1 | Structural framework

Figure 1 highlights the key structural elements of the study area in the West Xylokastro and Evrostina region of the southern margin of the Gulf of Corinth. During the latter stages of Rift 1, the southern margin lay along the Mavro Fault, containing the Mavro Delta and the Amphithea Faults to the west (Gawthorpe et al., 2018). This margin was complicated by the presence of antithetic faults (the Vryssoules and Koutsa Faults), the footwall of which generated a positive topographic feature. At the onset of Rift 2 (~1.5 Ma), this margin had migrated northward, with strain localised on the West Xylokastro Fault. The growth of the West Xylokastro Fault led to the continued development of the Xylokastro Horst, bound by the West Xylokastro Fault and the Vryssoules and Koutsa Faults, with some minor structures generating an intra-horst graben. The Xylokastro Horst comprises Mesozoic basement limestones of the Pindos and Tripolis and the Ano Pitsa and Korfiotissa Formations of the earliest part of Rift 1 units (Gawthorpe et al., 2018; Rohais & Moretti, 2017; Skourtsos & Kranis, 2009).

The West Xylokastro Fault forms a present day topographic escarpment of an exposed fault plane, showing the greatest relief (and displacement; >1 km) at its centre near the village of Ano Loutro (Figures 1, 2 and 3). The main phase of West Xylokastro Fault activity was from ~1.5 Ma to ~0.7–0.6 Ma (Ford et al., 2016; Gawthorpe et al., 2018). Dating of calcite cements show minor reactivations throughout the Late Pleistocene (Causse, Moretti, Eschard, & Micarelli, 2004; Flotté & Sorel, 2001). However, these were unlikely to be responsible for generating significant subsidence in the hangingwall, but may have allowed upward fluid migration, promoting the generation of perched tufa and travertine deposits in the immediate hangingwall, near Eliniko (Figures 1 and 2; Gawthorpe et al., 2018).

In its western portion, this displacement and escarpment dies out, with the fault tip likely buried by the Evrostini/Ilias fan delta system. The West Xylokastro Fault forms the co-linear fault array with the Valimi Fault in the west (Ford et al., 2016; Gawthorpe et al., 2018; Rohais, Eschard, et al., 2007; Rohais, Joannin, et al., 2007; Figure 1b). The relay between the West Xylokastro and Valimi faults is the site of the Evrostini/Ilias fan delta, which is dissected by several faults (Rohais, Eschard, et al., 2007; Rohais, Joannin, et al., 2007; Rohais et al., 2008; Zhong et al., 2018; Figures 1 and 2). Ford et al. (2016) interpret that these faults are likely not basement involved and instead reflect thinner-skinned (intra-Evrostini/Ilias) deformation of the sedimentary cover, which link at depth to a deeper-seated breach in the relay. The Evrostini Growth Fault, which hosts the Evrostini/Ilias fan delta system, shows significant back-rotation of the Evrostini delta topsets in its uppermost portion. We do not interpret that the Evrostini Growth fault directly links with the West Xylokastro Fault through a region of largely land-slipped exposures. Instead, we invoke the western toe of the Xylokastro Horst as a complex region of deformation by multiple minor faults in sedimentary cover accommodating the breaching of the relay at depth in agreement with Rohais, Eschard, et al. (2007); Rohais, Joannin, et al. (2007); Rohais et al. (2008) and Ford et al. (2016).

The WXFB, in the hangingwall of the West Xylokastro Fault, is bounded to the north by the presently active margin generated by the Derveni and Likoporiá Faults (Nixon et al., 2016). Offshore observations estimate that these faults became active ~0.75 Ma (Gawthorpe et al., 2018; Nixon et al., 2016). This is coincident with: (a) northward migration of fault activity in the west (Pirgaki-Mamousia Fault to the West Helike Fault (Ford, Williams, Malartre, & Popescu, 2007), (b) biostratigraphic constraints of the Vouraikos fan delta in the hangingwall of the Pirgaki-Mamousia Fault (Ford et al., 2007), and (c) beach deposits (MT on Figures 1b and 2) in the WXFB at an elevation of ~270 m that unconformably overlie deep-water sediments of the Rethi-Dendro Formation. Combined with uplift rate estimates from Armijo et al. (1996) of ~1.3–1.5 m/kyr we place this emergence of hangingwall stratigraphy at ~207–180 ka. Assuming their basal surface onto the underlying Rethi Dendro Formation was representative of the prior palaeobathymetry of water depths between 400 and 500 m, this is consistent with timings of activity on the Likoporiá and Derveni Faults from ~750 ka (de Gelder et al., 2019; Fernández-Blanco et al., 2019; Gawthorpe et al., 2018; Nixon et al., 2016). With the growth of the Derveni and Likoporiá Faults, the WXFB stratigraphy records a history as a relatively open rift margin and the transition ultimately to an uplifted fault terrace.

Within the WXFB, minor intra-basinal structures are present (Figures 1, 2 and 3), slightly oblique to the E-W trend of the West Xylokastro Fault, and aligned to the Likoporiá Fault. We interpret that this obliquity is caused by the

continued northward migration of strain onto the NNW-SSE oriented Likoporiá structures. Minor faults show cross-fault facies and thickness changes showing they were active during deposition producing variable basin floor topography. These structures (<30–50 m throw) have a weak expression and are either mapped on the basis of abrupt facies terminations (e.g. Minor Fault 1 in Figures 2 and S1) or from observation of offset layering in cliff faces, although their lateral continuity carries some uncertainty. The faults along the northern coastline are related to the Likoporiá and Derveni Faults, either as footwall splays or as part of a broader fault array. These faults are either blind and form a north-facing monocline in the very edge of exposures near the village of Stomio (Figure 2), or host the Late Pleistocene Rhodea Delta in their hangingwall. Zhong et al. (2018) propose the existence of N-S oriented transfer faults in the WXFB. However, we observe complete stratigraphic continuity and an absence of deformation in the N-S orientated perched river valleys that they attribute to such structures. Zhong et al. (2018) identify a change in facies across this valley, which we attribute to stratigraphic architectural variation (discussed in Section 4.3), rather than a post-depositional translation from N-S striking transfer faults. Whilst an underlying N-S oriented Mesozoic, Hellenic thrust sheet fabric underlies the Gulf of Corinth (Ford et al., 2016; Gawthorpe et al., 2018; Papanikolaou & Royden, 2007; Skourtsos & Kranis, 2009) we see no evidence to suggest reactivation and upward propagation of these features in the West Xylokastro area.

4.2 | Depositional elements

Given the scale and variability of the study area, depositional elements are used to describe the stratigraphy in each stratigraphic unit (Figure 4), and are only applied here to deposits in the bottomsets and basin-floor of the WXFB.

4.2.1 | DE1 – Mudstones and Marlstones

Description

DE1 comprises fine-grained intervals (1–30 m thick) of mostly grey-buff calcareous mudstones (marls), which are rarely black or organic rich. Except for gastropod and brachiopods within the Evrostini/Ilias delta, mudstones are largely non-fossiliferous. Mudstones can appear in several forms:

1. Massive – absent or only very weak sedimentary layering.
2. Decametric layered with red horizons – generally comprising massive or mm-laminated, fissile grey, mud-rich siltstones with 1–5 mm dark brown/red horizons spaced every few ~10 cm. Typically, these horizons are harder than the surrounding siltstones and locally are pyritised.
3. Decametric layered with sandstone beds – cream or grey mud-rich siltstones with rare dark grey- pale brown, normally graded sandstone beds (1–5 cm thick). Weak to moderate bioturbation (base of normally graded sandstones), restricted to *Planolites* and *Chondrites*.
4. Laminated – mm-laminated mud-rich siltstones, typically fissile/soft alternating between dark grey and brown-red in intervals of 5–10 cm. Bioturbation is not apparent at outcrop. Very rare current ripples.

Interpretation

Mudstone intervals are interpreted as fringe deposits or representing times of reduced sediment delivery to the basin, possibly with minor components of hemipelagic or hemilimnic fallout. The absence of black, organic-rich mudstones is attributed to the delivery of thin, dilute turbidity currents, represented by graded beds, which oxygenated waters in the deeper basin. This is supported by bioturbation, although the low ichnofacies diversity reflects strained seafloor populations.

4.2.2 | DE2 – Convex-up bodies (CUBs)

Description

Convex-up bodies (CUBs; 300 m wide and 25–30 m thick) observed in the bottomsets of the Ilias delta mainly comprise pebble-grade conglomerates, and are internally stratified (1–10 m scale; Figure 5). Clast sizes range from small pebbles to boulders, with limestone, chert, metamorphic and sedimentary extrabasinal clasts and silt/mud intraclasts up to 0.5 m in diameter. Flame structures, injectites, and <2 m offset, synsedimentary faults occur immediately below the CUBs disturbing their otherwise flat bases. The long axes of CUBs are parallel to nearby erosional bedforms (e.g. Xelidori Scour, Figure 6). The CUBs are recognizable by semi-radial dips and a convex upper surface forming a lobate geometry. The conglomeratic core is disturbed by dewatering structures and 1–2 m wide scours. Away from the axis, beds are dominated by chaotic, massive clast- and matrix-supported conglomerates. Toward the fringes, beds are increasingly cross-stratified, with normally and inverse graded pebbly sandstones (0.5–1 m thick) interbedded with packages of plant-rich siltstone and mudstones (~0.3–1 m thick). Typically, the matrix comprises very fine sand to gravel and is poorly sorted.

Interpretation

The stratification in these CUBs supports a composite origin. The poorly sorted, chaotic character of conglomerates supports a debrite interpretation. The absence of clays means that the flows may have exhibited frictional or very weak cohesive behaviour during their depositional stage. Graded gravelly/pebbly sandstones in the fringes of the CUBs are interpreted as granular flows and high-density turbidites (Lowe, 1982) intercalated with low-density siltstone and mudstone turbidites. The fringes may be the

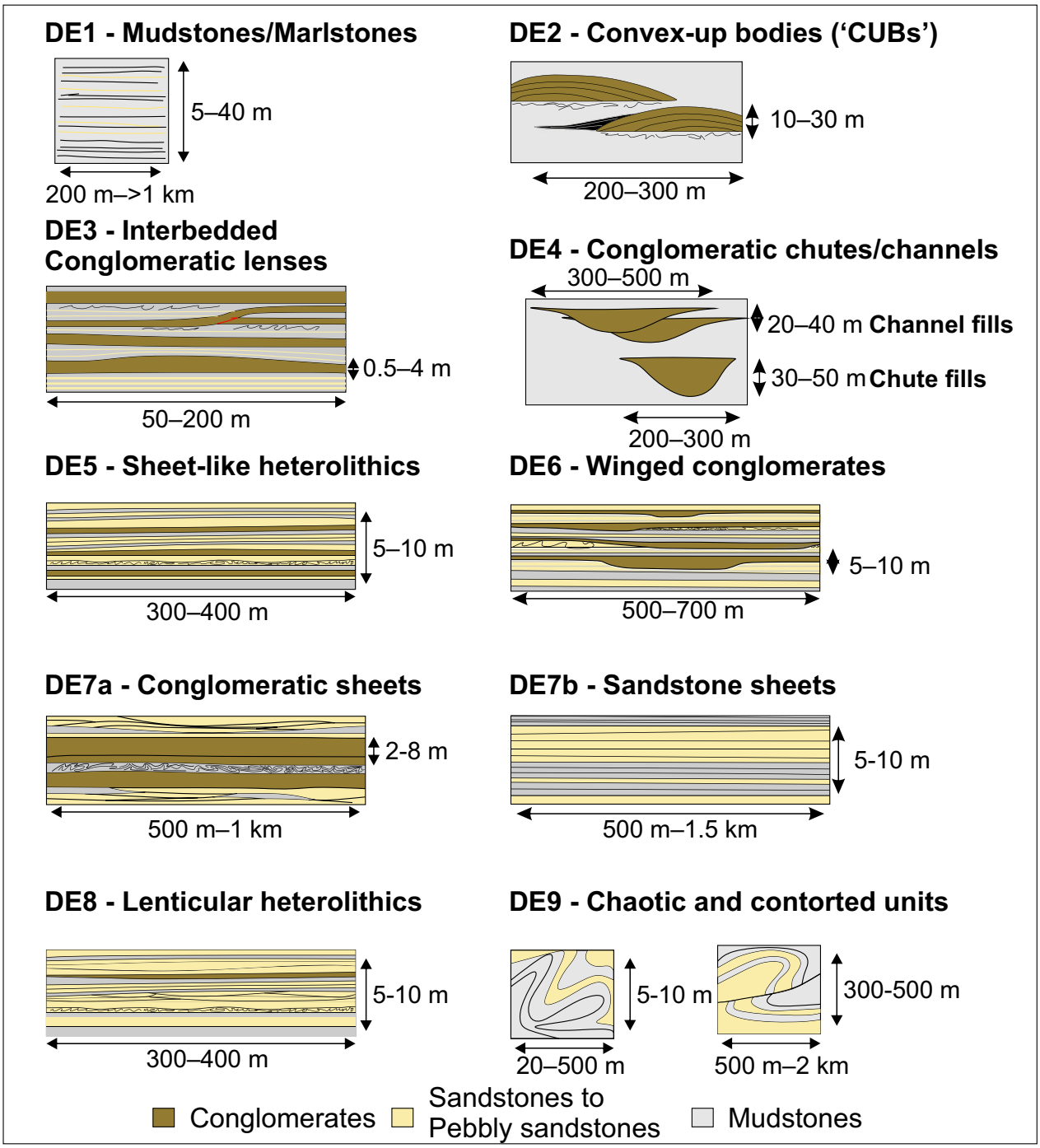

FIGURE 4 Summary of depositional elements used to describe stratigraphy in the study area

distal/lateral equivalent of the conglomeratic parts of the CUBs representing the transformation of originally conglomeratic flow, although outcrop limitation prevents confident bed-scale correlation.

The CUBs in the Ilias bottomsets are interpreted as coarse-grained base-of-foreset lobes, similar to those described as 'sandy lobes', 'fjord bottom splays', or 'tongues' in bathymetric datasets of deltaic systems (Kostaschuk & McCann, 1989; Postma & Cruickshank, 1988; Prior & Bornhold, 1988; Prior, Wiseman, & Bryant, 1981). This interpretation is supported by their position downdip of conglomerate-filled megascours, and incorporation of large sedimentary intraclasts. Disturbed and scoured central portions show characteristics of 'jet' expansion (sensu. Hoyal et al., 2003), where flows abruptly exit a confined setting (e.g. a chute) in the foreset to bottomset transition. The basal deformation suggests deposition onto a weak, mud-rich substrate.

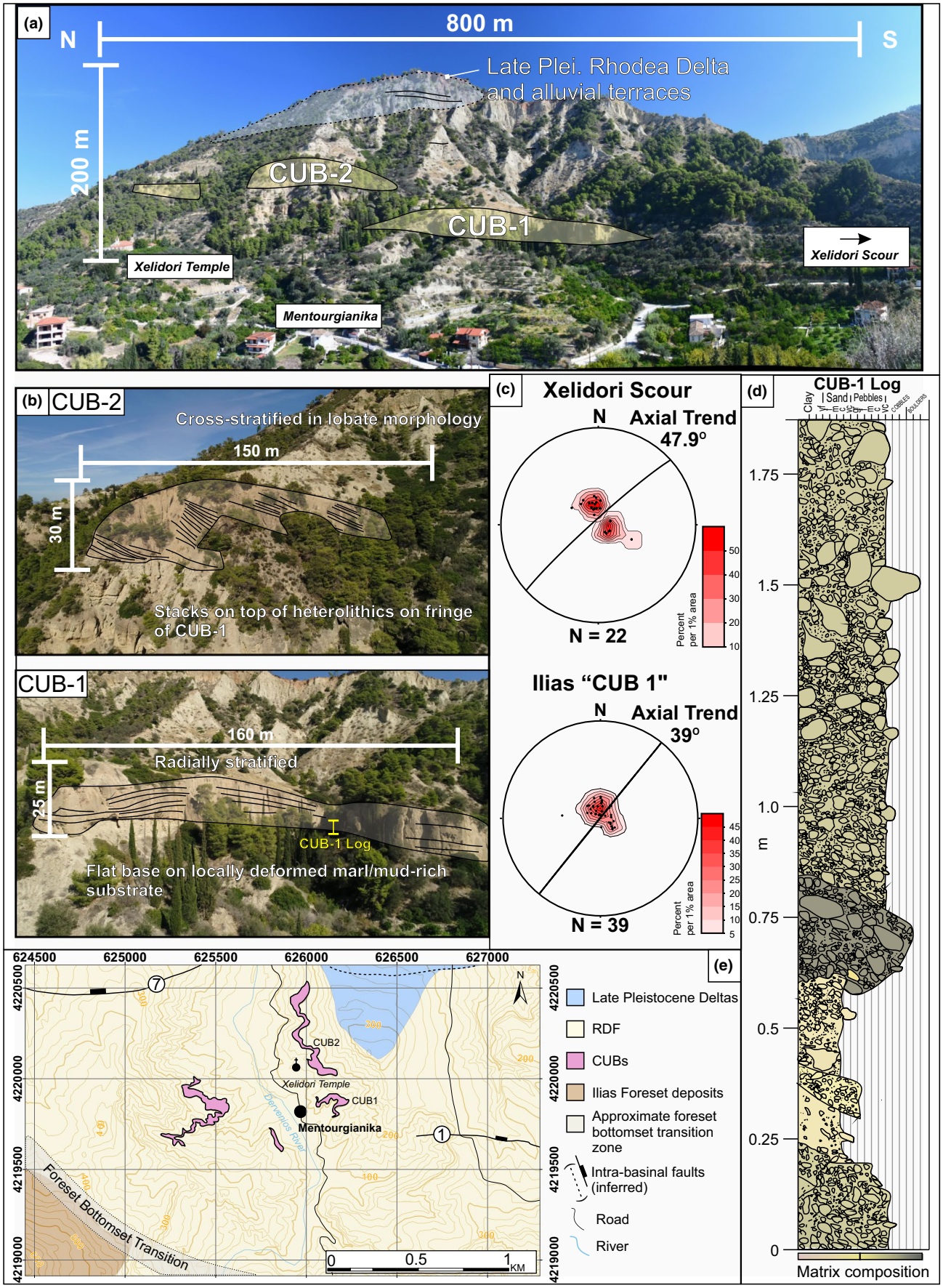
(a)
N
800 m
S
Late Plei. Rhodea Delta
and alluvial terraces
200 m
CUB-2
CUB-1
Xelidori Temple
Xelidori Scour
Mentourgianika
(b) CUB-2
Cross-stratified in lobate morphology
150 m
30 m
Stacks on top of heterolithics on fringe
of CUB-1
CUB-1
160 m
Radially stratified
25 m
CUB-1 Log
Flat base on locally deformed marl/mud-rich
substrate
(c)
Xelidori Scour
N
Axial Trend
47.9°
N = 22
Percent
per 1% area
Ilias "CUB 1"
N
Axial Trend
39°
N = 39
(d)
CUB-1 Log
Clay
Sand
Pebbles
COBBLES
BOULDERS
m
Matrix composition
624500
625000
625500
626000
626500
627000
4220500
4220000
4219500
4219000
CUB2
Xelidori Temple
CUB1
Mentourgianika
Foreset Bottomset Transition
0
0.5
1
KM
(e)
Late Pleistocene Deltas
RDF
CUBs
Ilias Foreset deposits
Approximate foreset
bottomset transition
zone
Intra-basinal faults
(inferred)
Road
River

FIGURE 5 (a) Overview of the locality of the cliffs behind the village of Mentourgianikia and the Xelidori Temple showing the forms of two 'CUBs'. (b - upper) Close up UAV photograph of CUB2 showing the development of cross-stratification and stacking onto a heterolithic fringe of CUB1. (b - lower) UAV photograph of CUB1 showing a strike-oriented section of a CUB form that highlights the radial style of bedding and flat base at the element scale. (c) Lower hemisphere stereonets showing the agreement of axial trends of CUB1 in agreement with the Xelidori Scour (Figure 6e). Black dots are poles to bedding with a calculated great circle describing an axial plane. Measurements made from a digital outcrop model using LIME. (d) Sedimentary log demonstrating the typical conglomeratic deposits of CUB-1. (e) Inset map (location provided on Figure 2) highlighting the location of CUB outcrops with respect to the foreset-bottomset transition of the Ilias delta

4.2.3 | DE3 – Interbedded conglomeratic lenses

Description

Conglomeratic lenses in the bottomsets of the Ilias delta have a high aspect ratio and convex-up morphology (50–200 m long, 0.5–1 m thick; Figure 6b). Conglomeratic lenses comprise both matrix- and clast-supported conglomerates, with high concentrations of sub-rounded to well-rounded small pebbles to rounded-subangular large cobbles with a poorly sorted muddy to coarse sand matrix. Typically, clast distribution is chaotic or massive, although locally beds show normal or inverse grading, and stacked clast imbrication with long-axes parallel to palaeoflow recorded in surrounding finer-grained deposits. Clasts are dominantly limestone, with subordinate chert, metamorphic, sedimentary extraclasts, typical of Evrostini/Ilias drainage assemblages (Gawthorpe et al., 2018). Conglomeratic lenses intercalated with massive/structureless medium sandstones and bedsets (0.2–2 m thick) of siltstone and climbing ripple laminated sandstone form fining up successions. Finer grained bedsets thin over conglomerate lenses. Isolated gravel and cobble clasts on bed contacts are common in fine-grained bedsets. Convolute bedding and intra-formational northward verging thrust faults are common in fine grained bedsets. Locally, muddy-siltstones contain disarticulated and broken shelly fauna.

Interpretation

The conglomeratic lenses show characteristics typical of debrites, although they could be attributed to a broad spectrum of gravity current behaviour, from cohesive (i.e. mud-rich matrix) debris flows to flows transitional between debris flows and granular flows (Gobo, Ghinassi & Nemec, 2014; Lowe, 1982). Sandstones and mudstones are interpreted as dilute, low-density turbidites, either as the tail of bypassing flows, or flows deficient in sand and gravel. Sediment bypass is supported by isolated extrabasinal clasts at bed contacts (Stevenson, Jackson, Hodgson, Hubbard, & Eggenhuisen, 2015). The geometry (Figure 6b) of conglomeratic lenses is consistent with a barform in the immediate bottomset position. Convolute bedding and intraformational faults resulted from mass movement of the foreset.

4.2.4 | DE4 – Conglomeratic channels and chutes

Description

In depositional strike sections in the immediate bottomset region of the Ilias delta, chaotic conglomerate-filled, concave-up lenticular bodies (DE4; 40–90 m wide, 20–35 m thick; Figure 6) overlie erosion surfaces that incise into fine-grained marlstone deposits. Internally, they comprise cobble-grade matrix- and clast-supported conglomerates with sedimentary intraclasts, in discontinuous or amalgamated beds (0.5–3 m thick). Rounded to sub-angular clasts range from small pebbles to small boulders. Rare thin (0.15–0.3 m thick) and laterally discontinuous poorly sorted sandstone horizons (<1–2 m long) are observed, occasionally containing pebble sized mud intraclasts. Distally (~7 km from the Ilias delta, near Skoupeikia/Kalithea at the locations later described in Figures 8 and 13c) higher aspect ratio conglomerate-filled bodies (20–40 m thick, 300–500 m wide) comprise stacked tabular beds.

Interpretation

The lenticular bodies are interpreted as channel-fills with geometries and dimensions similar to chutes reported from bathymetric datasets on modern delta foresets and bottomsets (e.g. Kostaschuk & McCann, 1989; Prior et al., 1981). They are likely formed by erosive flows that left behind coarse-grained lag deposits.

4.2.5 | DE5 – Sheet-like heterolithics

Description

Sheet-like heterolithics, one of the most common depositional elements found in the WXFB, comprise 5–10 m thick packages that extend laterally with limited thickness change over 300–400 m. They comprise massive gravel-rich or normally graded coarse to fine sandstones (0.3–0.8 m thick beds), and can contain conglomeratic or pebbly sandstone horizons. Gravelly sandstones can contain pebble-sized, angular mud-intraclasts at their base, or dispersed throughout the bed. Interbedded current ripple-laminated siltstones, normally graded medium to very fine sandstones, and deformed mudstones are common.

Interpretation

Sheet-like heterolithics encompass the deposits of high-density, gravelly/pebbly turbidity currents, sand-rich

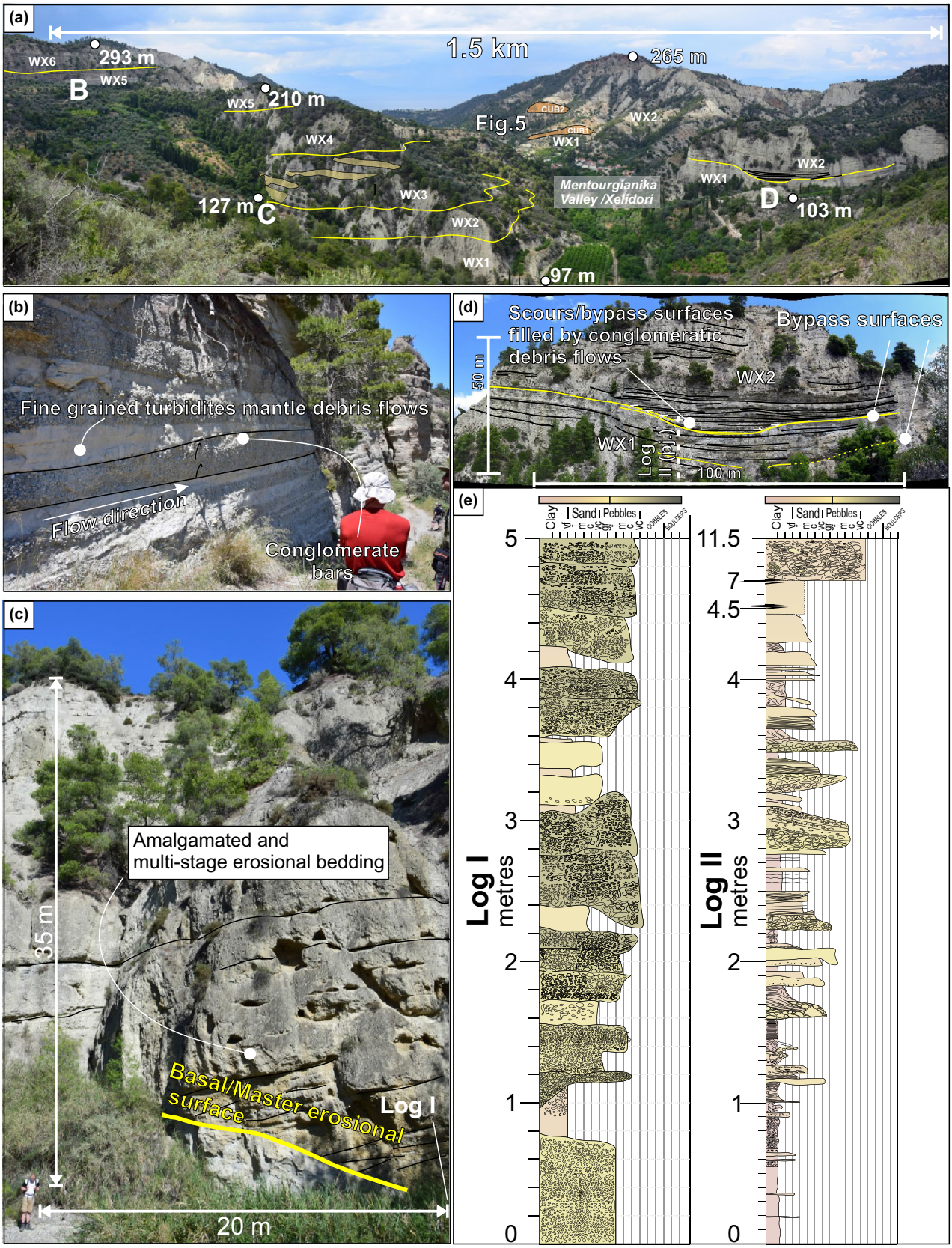

FIGURE 6 (a) Lookout point showing the proximal bottomset region in the Mentourgianikia Valley showing a variety of depositional elements and unit distinctions (described in Section 4.3). Letter labels refer to the location of figures below. (b) Interbedded conglomeratic lenses, DE3 in the bottomset of the Ilias delta. (c) Conglomeratic chutes in the bottomset of the Ilias delta (DE4). (d) Scour surfaces common within complex heterolithic intervals (DE8) in the bottomset. This particular example is herein termed the 'Xelidori Scour'. (e) Example logs comparing the infill of scours (I) and chutes (II). Log II is projected from exposures behind the cliff shown in (d)

transitional and debris flows and the dilute tails of turbidity currents (Cronin, 2018; Lowe, 1982; Sumner, Talling, & Amy, 2009). We interpret these deposits to represent proximal off-axis or medial, lobes, or apron sedimentation dominated by sand-rich to gravelly, weakly or non-confined gravity currents in the proximal-medial part of bottomset and basin floor fans (Cronin, 2018; Henstra et al., 2016). Conglomeratic layers and the lack of clear coarsening- and thickening-upward cycles likely represent fluctuation in sediment flux or autogenic variations (MacDonald, Peakall, Wignall, & Best, 2011).

4.2.6 | DE6 – Winged conglomerates

Description

Laterally-extensive conglomerates (Figure 7) have undulose bases, with a thicker (~0.5–1.5 m), locally erosive-based central portion, and thicken and thin laterally over ~500 m, in response to underlying contorted and deformed deposits. The edges of some conglomerates contain inclined surfaces that can drape and expand from surfaces that overlie the margins. Typically, the conglomerates comprise moderately to poorly sorted, sub-rounded to sub-angular pebble-cobble grade conglomerates in a poorly sorted sand-rich matrix. Conglomerate extraclasts are limestones, with subordinate phyllites, cherts and sedimentary clasts, and up to boulder-sized mud-intraclasts.

Interpretation

The process responsible for the deposition of these conglomerates is interpreted to be highly concentrated (debris) flows (Cronin, 2018; Postma, 1986; Lowe, 1982). The winged geometry is attributed to flows that were initially focussed into topographic lows above rugose debrite and slump relief, which spilled and expanded as the depositional topography healed. Inclined stratification at the lower margins of these bodies are interpreted as lateral accretion surfaces/bars, which occur in combination with overall thickness changes (Kane, Dykstra, Kneller, Tremblay, & McCaffrey, 2009). The environmental setting was dynamic, with abrupt changes between 1–2 m thick conglomerates and successions of finer grained intervening deposits representing much lower sedimentation rates, interrupted by episodic slump and slide events.

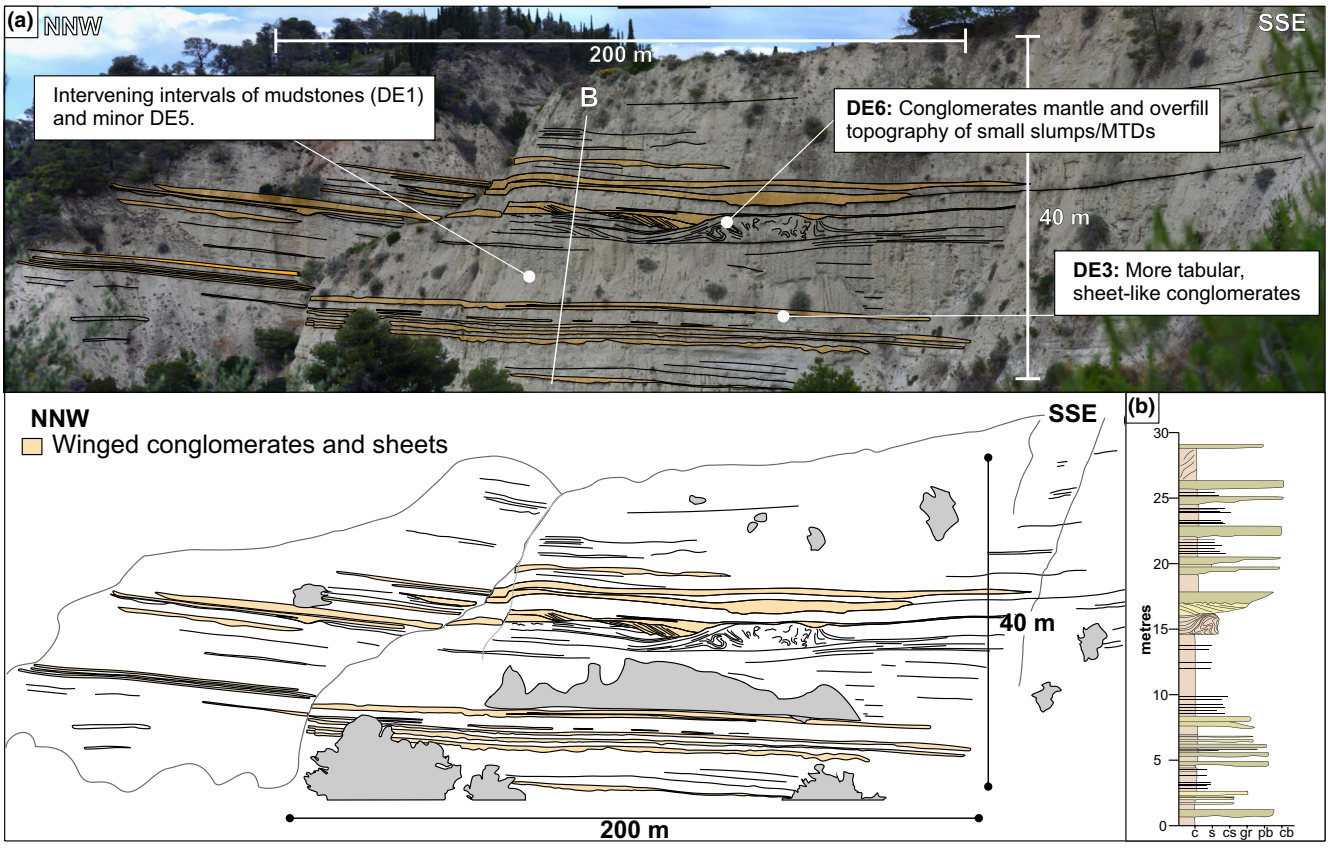

FIGURE 7 (a) Outcrop photopanel and sketch of cliffs to the north of Ligia viewed from the road to Pyrgos showing the development of winged, conglomeratic bodies (DE6) mantling the topography generated by small discontinuous slumps (DE9). Viewing direction is towards the NE. (b) Sketch-log for location shown in (a), thickness measurements of units confirmed with digital outcrop model

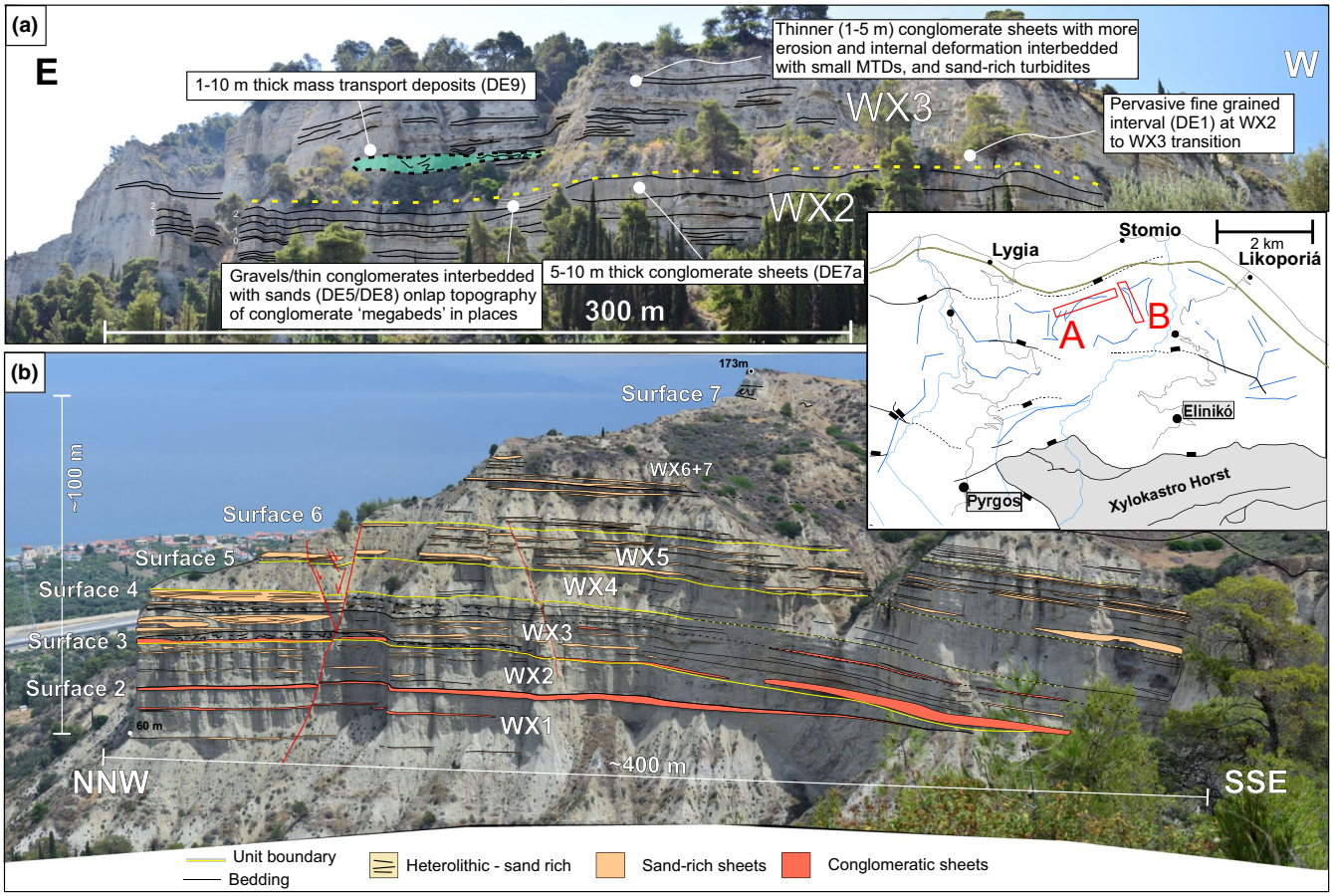

FIGURE 8 (a) Photograph showing an approximate dip section of cliff faces near the village of Stomio that present laterally continuous composite conglomeratic sheets (DE7a) interbedded with sand-rich and frequently scoured intervals, common in the distal bottomset (DE5 and DE8). Green deposits are slumps (DE9). (b) Strike-section through exposures of the distal bottomsets between the village of Stomio and Skoupeikia/Kalithea. Coarse-grained bodies are highlighted with intervening stratigraphy generally comprising heterolithic, but mud-rich facies

4.2.7 | DE7a – Conglomeratic sheets

Description

Conglomeratic sheets (2–8 m thick) are 0.5–1 km long and ~0.5 km wide, and tend to have sharp, non-erosional bases, and uneven tops that grade into deformed heterolithic to sand-rich portions (Figure 8). Typically, the conglomerates are clast-supported, with matrix-supported portions, containing large pebbles and cobbles and rare small boulders (30–40 cm diameter). Conglomeratic sheets appear amalgamated, although locally well-developed metre-scale cross-stratification is picked out by variations in clast concentration. The conglomeratic sheets are separated by either thin (<1 m) mud-rich successions, or thicker (1–5 m thick) sandstone-dominated heterolithic successions (DE5/DE8), and are commonly observed immediately downdip of winged conglomerates.

Interpretation

Conglomeratic sheets are interpreted as the deposits of hyperconcentrated flows and debris flows. Typically, they appear as a single discrete deposit, although cross-stratification at the edges suggests some are constructed by multiple events amalgamated at the axis. Overlying heterolithic to sand-rich upper divisions are interpreted to represent deposits from cohesive flows, similar to mud-rich contorted tops of hybrid flows (Bozetti, Cronin, Kneller, & Mark, 2018; Haughton, Davis, McCaffrey, & Barker, 2009). The sheets are interpreted as the proximal and axial parts of subaqueous lobes. The spatial transition from erosional-based, winged conglomerates into conglomeratic sheets suggests these may have formed in localities where flows underwent hydraulic jumps.

4.2.8 | DE7b – Sandstone sheets

Description

Tabular bodies (0.2–0.5 m thick) comprise amalgamated, massive to weakly normally graded medium-fine sandstones observed in cliff faces as proud-weathering coarse-grained ridges (1–10 m thick). Normally graded sandstones show well-developed planar lamination and current ripple lamination at bed tops, which either grade into convolute laminated mud-rich bed caps, or form abrupt grain-size breaks to

normally graded mudstone caps (~0.1–0.2 m thick). Angular, small to large pebble-sized mud chips are common. Rare coarsening- and thickening-upward trends are separated by mudstone intervals (DE1) and sheet like heterolithics (DE5).

Interpretation

Sandstone sheets are interpreted as deposits of sand-rich turbidity currents and muddier hybrid or transitional flows (Haughton et al., 2009; Kane, Pontén, Vangdal, Eggenhuisen, & Hodgson, 2017; Lowe, 1982). Tabularity and lateral extent suggests deposition in a weakly confined setting where flows expanded laterally and are interpreted as the medial to distal parts of lobes in basin floor fans (MacDonald et al., 2011).

4.2.9 | DE8 – Lenticular heterolithics

Description

Sandstone- and gravel-rich successions that comprise lenticular bodies, which overlie and are cut by scours, forming bedsets 5–10 m thick and 100–300 m long. Scour surfaces can be draped by mudstones and fine sandstones, and are passively onlapped by conglomeratic beds. Sandstones/gravelly sandstones contain large pebble/boulder-sized sedimentary intraclasts and multiple internal erosion and amalgamation surfaces. Intercalated finer grained units comprise interbedded tabular sandstones and siltstones, and rare mudstone/marlstone units (~1–5 m thick).

Interpretation

DE8 is interpreted to characterise areas prone to scouring, such as base-of-slope or very proximal parts of lobes. Scour surfaces mantled by mudstones and sandstones represent the finer grained tails of largely bypassing flows. Where these flows are not bypassing and/or partly confined they deposit as conglomeratic debrites infilling scours. Minor laterally pervasive (10s of metres) mud-rich intervals reflect periods of relative quiescence (e.g. Strachan et al., 2013). Large sedimentary intraclasts in sandstone suggest proximity to updip erosional features, such as chutes or minor channels.

4.2.10 | DE9 – Chaotic and contorted units

Description

DE9 includes a range of highly deformed and laterally extensive deposits that are largely mudstone rich but are highly variable and heterolithic with up to conglomeratic megaclasts or competent horizons. DE9 is subdivided into two principal end members:

A Sub-decametric to decametric-scale, deformed heterolithic units that range from well-developed sheath folds with traceable internal stratigraphy to entirely disaggregated with 10 m diameter megaclasts

B Kilometric-scale deformed stratigraphy northward verging sheath folds and thrust faults with large throw (>50 m).

Interpretation

Chaotic and contorted units are interpreted to represent a range of mass transport deposit (MTD) depositional processes ranging from large (kilometres wide by 100s of metres thick) coherent, slides through intermediate (100s of metres long by 10s of m thick) slumps and debrites, to small (<1 m thick) slumps and debrites. These mud-rich MTDs were likely sourced through remobilization on adjacent steep slopes.

4.3 | Definition of stratigraphic units

The ~800 m thick West Xylokastro RDF stratigraphy is split informally into a Lower and Upper Sub-Formation (Figure 2) to separate key areas of exposure constraint and stratigraphic differences explained herein. The clast assemblage data support an Ilias (Olvios drainage) source area (Gawthorpe et al., 2018; Rohais, Eschard, et al., 2007). We subdivide the stratigraphy further into 10 units, numbered WX1-WX8, plus the Pyrgos Member and the Likoporiá Slide, using regionally correlated stratigraphic surfaces, lithological or architectural differences, and dip projection along and between cliff sections (Figures 2, 3 and 9). Structural and stratigraphic mapping (Figure 2) shows that some units can be mapped from the Ilais delta foresets (Figure 10) 8–9 km downdip in a basin-axial fairway, as defined by palaeocurrent data (Figure 9 and Gawthorpe et al., 2018). We characterise spatial domains with respect to the base of the Evrostini/Ilias delta foresets, which geometrically define a break-in-slope. 'Proximal' describes a 0–2 km tract from the base of the Ilias foresets, 'Medial' from 2–5 km, and 'Distal' from >5 km of the base of foresets before a basin floor ~6–7 km from the base of the foresets. These units and their correlation are summarised in Figure 9. We also identify a transverse system (e.g. Figure 3b), limited to 1–2 km from the immediate West Xylokastro Fault scarp. This system is interpreted to be distinct based on: (a) northward verging thrust faults and sheath folds within mass transport deposits in this region, (b) minor occurrences of conglomerate assemblages in fault-proximal locations unlike Ilias assemblages (i.e. deficient in metamorphic clasts), and (c) spatially limited chaotic boulder clast rock-fall type deposits and chaotic/massive mudstones, typical of fault-scarp apron systems (Henstra et al., 2016; Sharp et al., 2000; Strachan et al., 2013) in the immediate hangingwall area. These are identified on Figures 2 and 3 as the 'Western Transverse System' (WTS), 'Central Transverse System' (CTS), and 'Likoporiá Slide'. The Upper WX and Pyrgos Members form part of latter stage uplift of the system, which is not the primary focus of this study and so are only described in their assistance to the mapping of structures and stratigraphy.

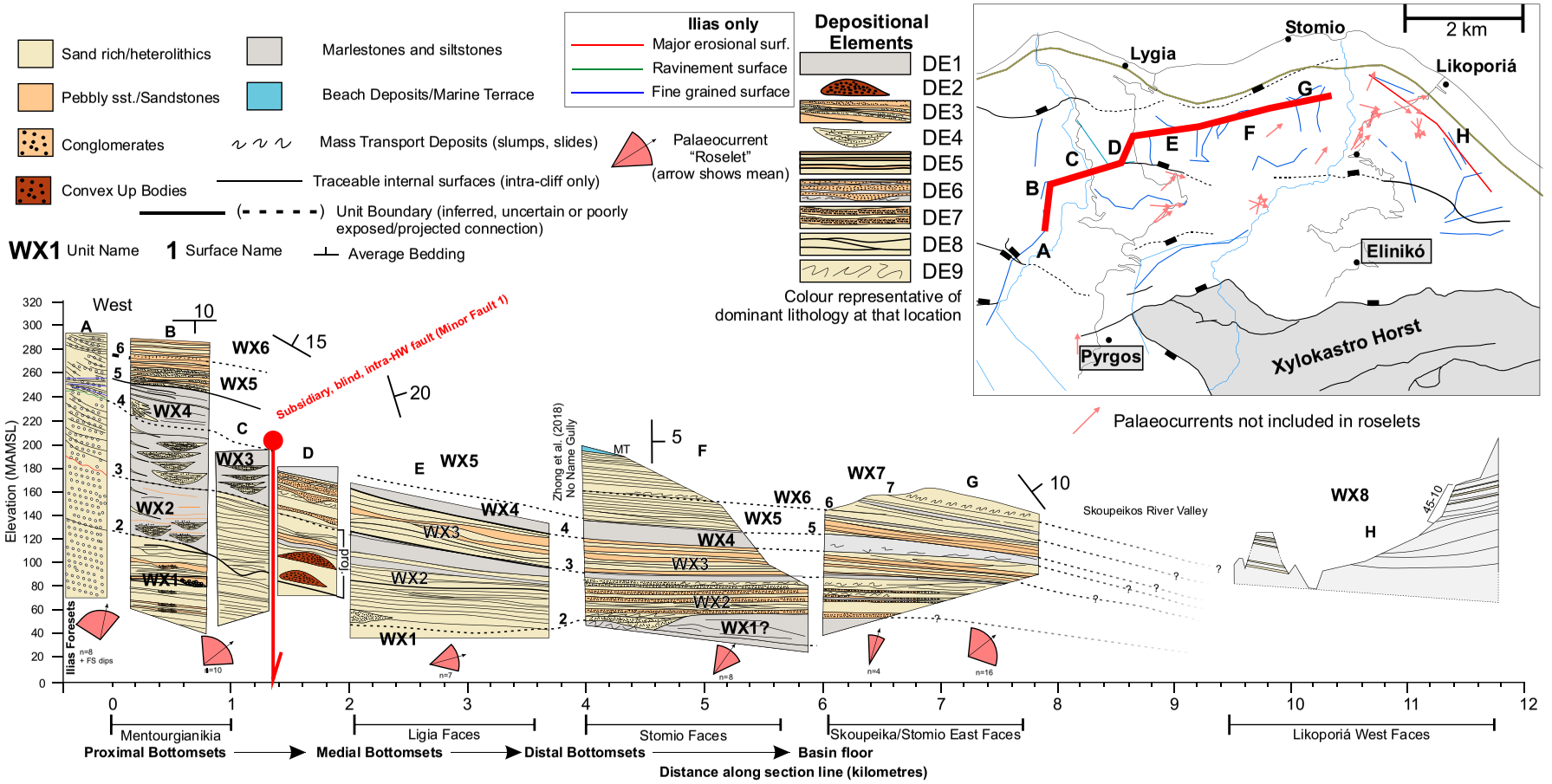

FIGURE 9 Composite correlation panel cartoon compiled from outcrop observations and projections through the WXFB. Palaeocurrent roselets are generated as a composite of all measurements from data within 300 m of the correlation line. Architectural forms are not to scale and are larger for clarity. Correlatable surfaces into the Ilias foresets are labelled. N.B. Surface 6 is equivalent with the 13 Surface in Rubi et al. (2018). Average dips are shown by bedding indicators, with N as the top of the figure

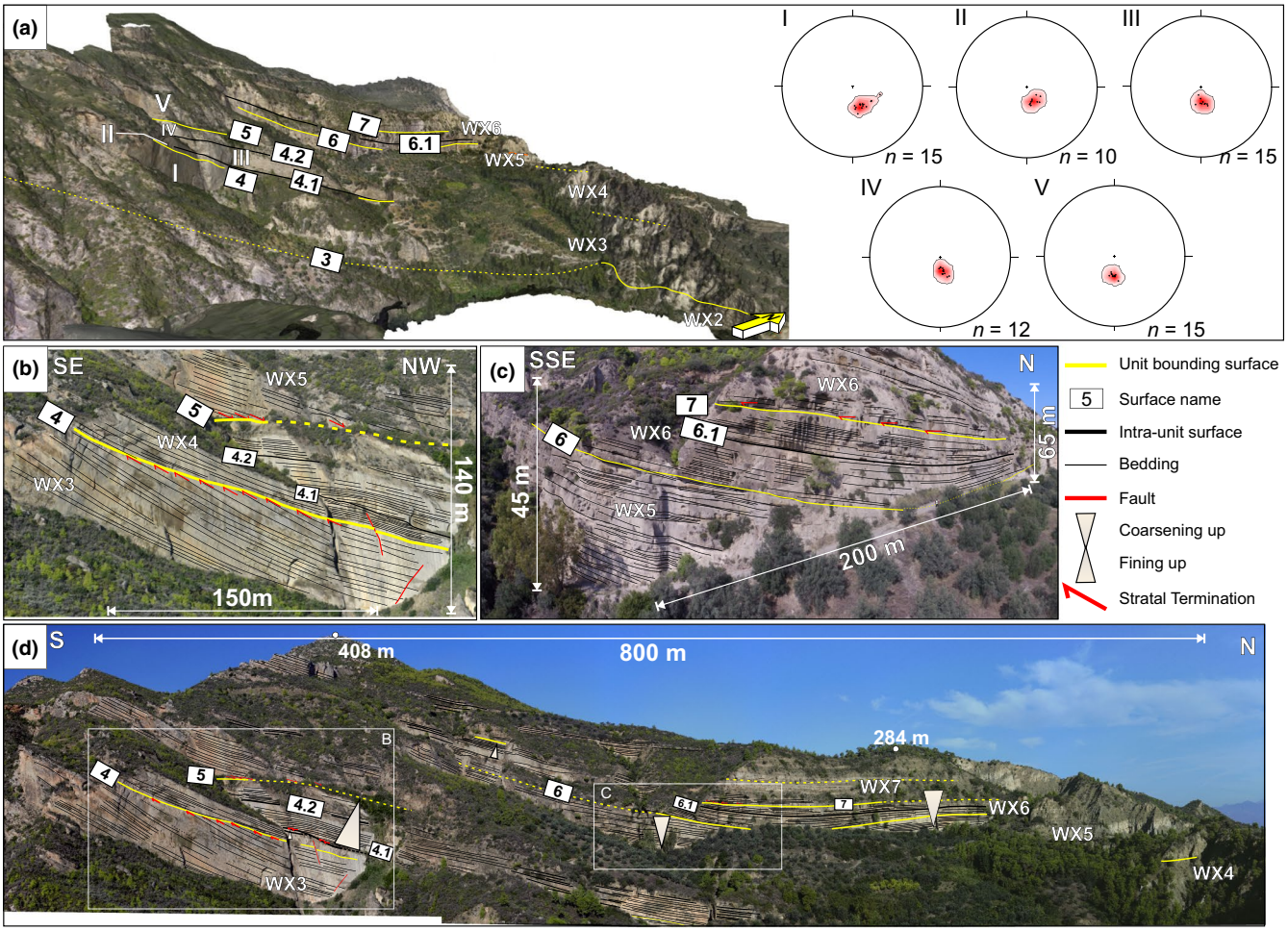

FIGURE 10 Overview of correlations of key stratigraphic surfaces in the Ilias delta foresets to bottomset units. (a) Digital outcrop model showing key unit bounding and intra-unit surfaces. Stereonets (located by white roman numerals on the model) measure foreset dip showing a progressive rotation from NW dipping 1 to NNE dipping 5 through an approximately 1D section. All are lower hemisphere projections showing poles to bedding. (b) Zoomed-in photograph highlights Surfaces 4–5 showing stratal termination styles in association with the development of WX4. (c) UAV photograph showing the stratal architecture in the foreset-bottomset transition in WX5 and WX6. (d) Overview photograph of Ilias delta foreset to bottomset transition showing key statal surfaces, bedding relationships and outcrop extents for WX3 to 7

4.3.1 | WX1

The base of WX1 does not crop out. Proximally, WX1 typically comprises marlstones (DE1) with ~500–700 m wide packages of lenticular heterolithics that are gravel-rich (DE8) and sheet-like, sand-rich heterolithic deposits (DE5). More distally, WX1 comprises marlstones (DE1) with rare sheet-like heterolithic deposits or rare, thin (<1 m) conglomeratic sheets.

4.3.2 | WX2

We correlate WX2 over ~8 km downdip from the proximal region of the Ilias bottomsets (Figures 6 and 9). The basal bounding surface, Surface 2, is traceable at similar structural elevations in much of the Mentourgianikia Valley, and has three characteristic styles within the proximal bottomset:

(i) Numerous large (~10s of m wide, several m deep) scour-fills, such as the Xelidori Scour - Figure 6) forming a composite surface (e.g. Xelidori Channel in Trout, 1999; Ilias Channel Levee system in Rubi et al., 2018).
(ii) Subtle changes from heterolithic/gravel-rich WX1 to boulder clast, chaotic deposits infilling scours or chutes.
(iii) Basal surface of CUBs (Section 4.2).

Three kilometres downdip, distinct grain-size and architectural changes mark Surface 2, with large incision surfaces that incise into WX1 overlain by WX2 conglomeratic channels/sheets (panels E and F in Figure 9). Seven kilometres further downdip of the base of the Ilias foreset, Surface 2 is not exposed.

Proximally, WX2 is extremely variable and comprises sheet-like and scoured, sand-rich turbidites and gravelly and conglomeratic debrites (DE5 and DE8),

convex-up bodies (DE2) and minor, conglomerate-filled chutes (DE4). This variability occurs within a ~3 km^2 area (~1.5 km wide and ~2 km long) at the base of foresets, likely due to process variability (both spatially and temporally) along the foreset of the Ilias delta. There is no observable vertical trend in the arrangement of these depositional elements. In the medial domain, WX2 comprises conglomeratic and sand-rich sheets (DE7a, b), and sheet-like and complex heterolithics (DE5 and DE8). Here, the upper part of WX2 comprises a ~10 m interval of marlstone (DE1). In the transition between the medial and distal domains, WX2 comprises mudstones (DE1) and minor sand-rich heterolithic intervals (5–10 m thick), coincident with an increase in eastward dips to 10–15 degrees (Figures 2 and 9) in response to a minor, intra-basinal fault (Fault 1, Figure 2). In the distal basin floor domain, a change in the thickness of typical depositional elements occurs over ~500 m between panels E and F (Figure 9). Conglomeratic sheets become the main component, comprising at least 15 m of the lower part of the unit (Surface 2 is poorly defined distally), with the overlying ~10 m marlstone thinning to ~2–4 m. A minor element of WX2 in its distal portion are slumps and debrites (DE9), which are more common towards the centre of the depocentre, and are interpreted to form from fault scarp apron collapse from the south. The significant proportion of conglomeratic depositional elements are restricted to the hangingwall of, and downdip from, an intrabasinal structure, Minor Fault 1 (Figure 2).

4.3.3 | WX3

WX3 is bound at its base by Surface 3, which can be correlated from a 5 to 15 m deep erosion surface, overlain by massive conglomeratic foreset deposits (30–50 m thick; Figures 10 and S2) to an erosive surface overlain by conglomeratic chute-fills in the proximal bottomset (DE4, Figure 6c). Toward the medial bottomset (~2 km from the base of the foreset), Surface 2 is conformable with the marlstone package in the uppermost WX2, overlain by relatively thin (0.5–1.5 m) conglomeratic sheets (DE7a) of the basal part of WX3. The most distal expression of Surface 3, near the village of Skoupeikia (Figures 8 and 9), conformably separates a southward thinning WX2, and an overlying southward thickening WX3.

Typically, WX3 comprises various coarse-grained elements. Proximally, it comprises a 40–50 m stack of ~15–30 m thick conglomeratic chute-fills (DE4, Figure 6a,c) with minor slumps (DE9) in the east (1–5 m thick, ~100–200 m wide). In the medial domain, winged conglomerates (DE6) dominate WX3 (Figure 7), which overlie and locally incise small slumps (DE9) and mudstone/marlstones (DE1). The winged conglomerates abruptly fine 200 m basinward to sandstone-rich heterolithics (DE8) with scour-fills separated by minor (1–5 m thick) mudstone intervals (DE1). In this region, eastward dips increase in magnitude in response to Minor Fault 1 (Figure 2), before shallowing out where the stratigraphy changes abruptly to winged and sheet-like conglomerates (DE6 and 7a), sheet and lensoid heterolithics (DE5), and minor occurrences (<5 m intervals) of mudstones (DE1). Photogrammetric models reveal scour-fills (~10s of m wide and 1–5 m deep) overlying sandstone dominated elements (DE8). We interpret that the change in slope from Minor Fault 1 leads to a sediment bypass-dominated zone (sensu Stevenson et al., 2015) within WX2 and WX3 in this region. The break-of-slope towards the centre of Minor Fault 1 leads to the deposition of a thicker conglomeratic sheet succession in the Stomio cliff faces (Panel F, Figure 9). Here, laterally extensive mudstones between conglomeratic sheets are interpreted to represent periods of reduced coarser grained sediment supply to the distal bottomsets and basin floor in this region. The conglomerate sheets near Stomio (Panel F, Figure 9) fine and thin eastward near Skoupeikia/Kalithea where WX3 comprises sand-rich sheets (DE7b), lenticular heterolithics (DE8), and minor conglomeratic channels (DE4). Minor slumps and debrites become more prevalent and thicker toward the east/centre of the depocentre. Most conglomeratic depositional elements are restricted to the hangingwall of and downdip from Minor Fault 1 (Figure 2).

4.3.4 | WX4

WX4 is a regionally extensive marlstone-dominated unit. The lower bounding surface, Surface 4, in the bottomset is subtle, and represented by a transition into fine-grained stratigraphy. In the foreset of the Ilias delta (Figure 10), Surface 4 truncates underlying WX3 foreset deposits, and is locally downlapped by WX4 foresets. In this region it comprises two mudstone-dominated intervals (Surface 4.1 and 4.2) separating sandstone-dominated foreset packages (~10–15 m thick), with upward changes of dip direction in this region of the foreset from NW to N. WX4 in the immediate bottomset region is ~45–50 m thick. WX4 gradually thins eastward/distally to ~15 m recorded near Skoupeikia/Kalithea in the distal bottomset/basin floor. Further eastward minor slumps (DE9) are prevalent within WX4.

4.3.5 | WX5

WX5 is recognised in the Ilias delta conglomeratic and sand-rich foreset deposits that downlap onto Surface 5. In the bottomset, this surface correlates with a stratigraphic change from WX4 mudstones and marlstones, to conglomeratic and sand-rich WX5, although locally this surface is hard to identify due to the variability of WX5. Distally, WX4 tops many

cliff exposures so Surface 5 is not exposed, with the exception of cliffs near Skoupeikia/Kalithea (Figure 8b) where Surface 5 is marked by a change from mudstone-dominated WX4 to heterolithic WX5.

At the foreset-bottomset transition, WX5 is a ~15–20 m thick succession of interbedded conglomeratic lenses (DE3) and minor heterolithic intervals (DE8; Figure 6a,b). More distally, lenticular and sheet-like heterolithics (DE5 and DE8) comprise WX5, although exposure is limited.

4.3.6 | WX6

The base of WX6, Surface 6, is marked by an erosion surface in the proximal bottomset overlain by an increase in the proportion of conglomerates, and a change in the architectural style (Figure 10c,d). Packages of conglomerate are more stratified towards the top of WX6, and thin toward the foreset *and* downdip. In the eastern part of the proximal bottomsets WX6 comprises sheet-like, gravel and sandstone-rich heterolithics (DE5) that are locally incised by conglomeratic and sand-rich channel bodies (DE4). Where exposed distally, WX6 is overlain unconformably by a beach deposit near Stomio (Panel F, Figure 9). Near Skoupeikia/Kalithea, WX6 comprises ~3–5 m intervals of gravel or sand-rich heterolithics and sheet-like heterolithics (DE5 and DE8) interbedded with 5–10 m intervals of mudstones (DE1).

4.3.7 | WX7

Surface 7 is identified in the proximal bottomsets by underlying truncated steeply dipping massive conglomerates, and overlying onlap of massive, stacked conglomerates of WX7 (Figure 10c). This records the youngest stratigraphy seen in the proximal bottomsets, exposing a 30 m thick section of massive conglomerates (DE3), with an overall fining- and thinning-upwards trend.

Distally, near Skoupeikia/Kalithea, WX7 is distinguished from WX6 by the presence of a 5–10 m thick, 600 × 500 m mass transport deposit (Figure 11). This mass transport deposit varies from highly chaotic and disaggregated poorly sorted sandy mudstone with up to 2 m diameter boulders of conglomerate (Figure 11a), through more coherent folded, mud-rich stratigraphy with floating boulders, to normal faulted coherent stratigraphy (Figure 11b,c). Normal faulted domains are restricted to southern areas, whilst compressional and highly disaggregated domains are present at edges and northern domains (Figure 11c). We interpret this to represent a northward transport direction, from collapse of the fault scarp apron in the immediate hangingwall of the West Xylokastro Fault.

WX7 and WX6 mostly comprise sheet-like sandstones and sheet-like and lenticular heterolithics. In the southern portion of WX7, it is incised by channels of the Pyrgos Member by ~20 m.

4.3.8 | WX8

A 600 m wide area of no exposure across the Skoupeikos river valley prevents direct observation of the change in character from conglomeratic/gravel rich WX7 to tabular sandstone and mudstone-prone stratigraphy to the east of the river. Projection of dip east of the Skoupeikos River suggests this is above WX7 and given the change in character is considered a separate stratigraphic unit, WX8.

East of Skoupeikia, 'badlands' topography and vegetation dominates as a result of the more mud-rich stratigraphy. However, several coarse grained ridges/horizons (~10 m thick) are tracked between outcrops, which comprise sand-rich lobes (Figure 12). Figure 12 shows an overview of a terraced olive grove that allows access to the "SKOUP-1" lobe horizon. Finer grained deposits mainly comprising homogenous marlstones interspersed with thin sandy turbidites dominate the basal part of these exposures (1C2, 1H, 1C and 1B in Figure 12c). The upper part of these exposures (1D, 1G, 1F, 1E in Figure 12c) are coarser and dominated by amalgamated, gravelly, high-density turbidites, hybrid beds and debris flows (DE7b). Similarly in the "SKOUP-0" lobe (Figure 12d), tabular, amalgamated sandstone beds form packages (DE7b) interbedded with heterolithic intervals, which are 0.5–1 m thick (DE5, minor DE1). Thicknesses (~2–8 m), facies and nature of these features (tabular and rare thickening and coarsening up successions), are similar to lobe elements identified in the Ross Formation, Ireland, by MacDonald et al. (2011).

4.3.9 | Pyrgos Member

The proximal Pyrgos Member (Figures 2 and 13a,b), comprises a ~100 m thick succession of conglomerates. It is underlain by steeper dipping RDF stratigraphy separated by a surface interpreted as an erosive surface. This surface might have been a locus for later deformation, which may have enhanced this angular discordance. Close inspection of this surface across the study area is not possible given limited accessibility and variable quality of the exposure. Typically, the conglomerate beds (0.3–0.8 m thick) are massive, comprise small-medium pebbles, and can be clast- or matrix- supported with a poorly sorted, clay-silt-gravel matrix. Downdip, this surface projects ~3 km into NE-SW trending conglomeratic channel (~100 m wide and ~35 m thick, Figure 13b) near Skoupeikia/Kalithea and Vyiazinika (Figures 2 and 13c,d) filled with cobble/boulder grade conglomerate deposits from debris flows and hyperconcentrated flows. Many of these conglomeratic deposits (e.g. Figure 13d) show clast long-axis imbrication (Ap/Ai sensu Harms,

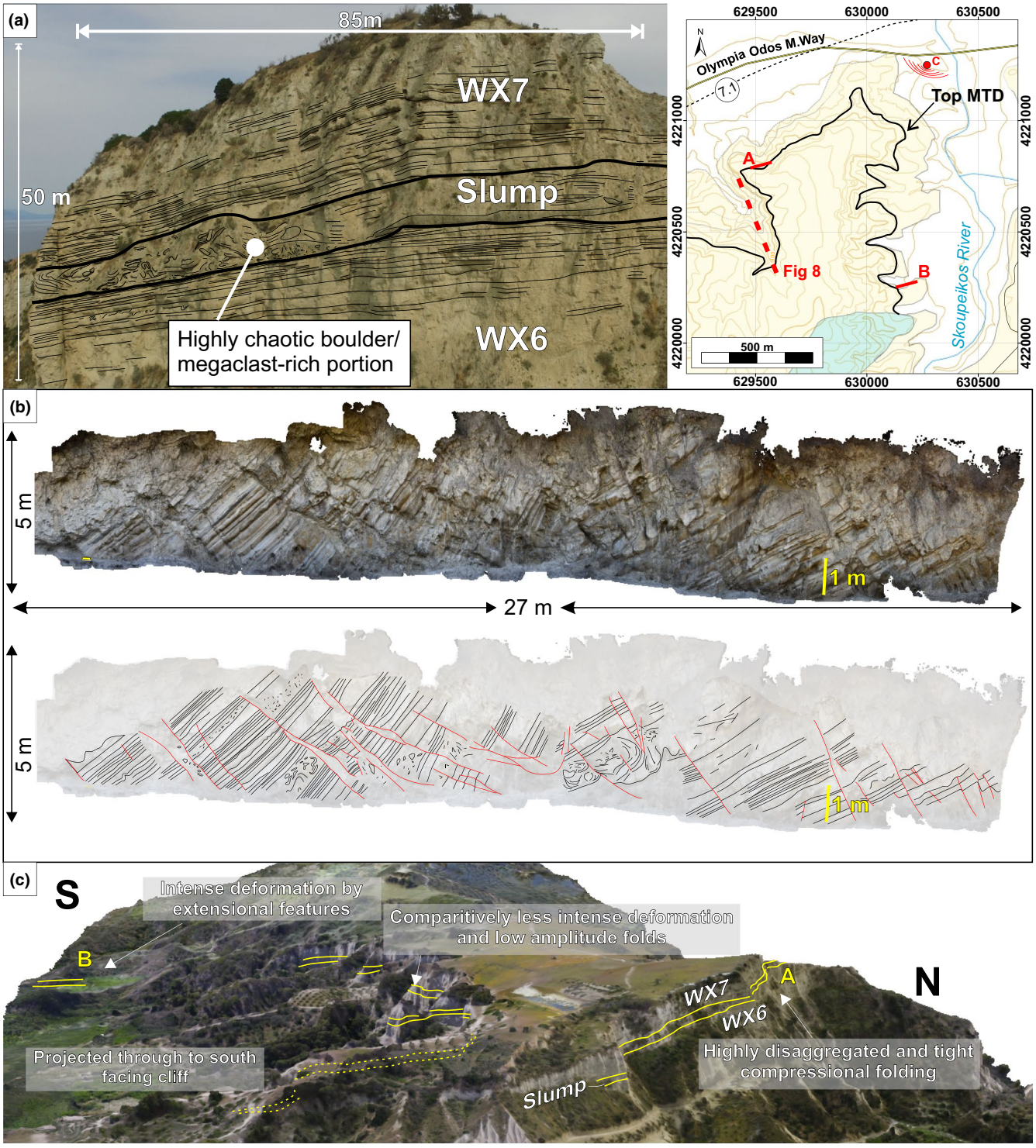

FIGURE 11 (a) UAV Photograph from the northern face of the Skoupeikia exposures highlighting the interbedded Slump which marks the base of WX7 in this region. The slump is highly chaotic and disaggregated and poorly sorted with and boulder sized conglomerate blocks. Top Right is an inset map for the locations within the figure. (b) Annotated photomosaic of the northern section of the same MTD body highlighting intense normal faulting. (c) 3D outcrop model view of the locations within 11a,b highlighting the spatial change in the style of deformation within the MTD at the base of WX7

Southard, Spearing, & Walker, 1975) in coarse sand-gravel matrices or have an open framework. Where this is the case, clast orientation can be treated as parallel to palaeoflow. Palaeoflow from clast imbrication in these beds (Figure 13d,e) is towards the NNE which is concomitant with the orientation of the Pyrgos Member and its exposed channel-fills (Figure 13). Clasts in the Pyrgos Member conglomerates comprise limestone, with subordinate cherts, sandstones

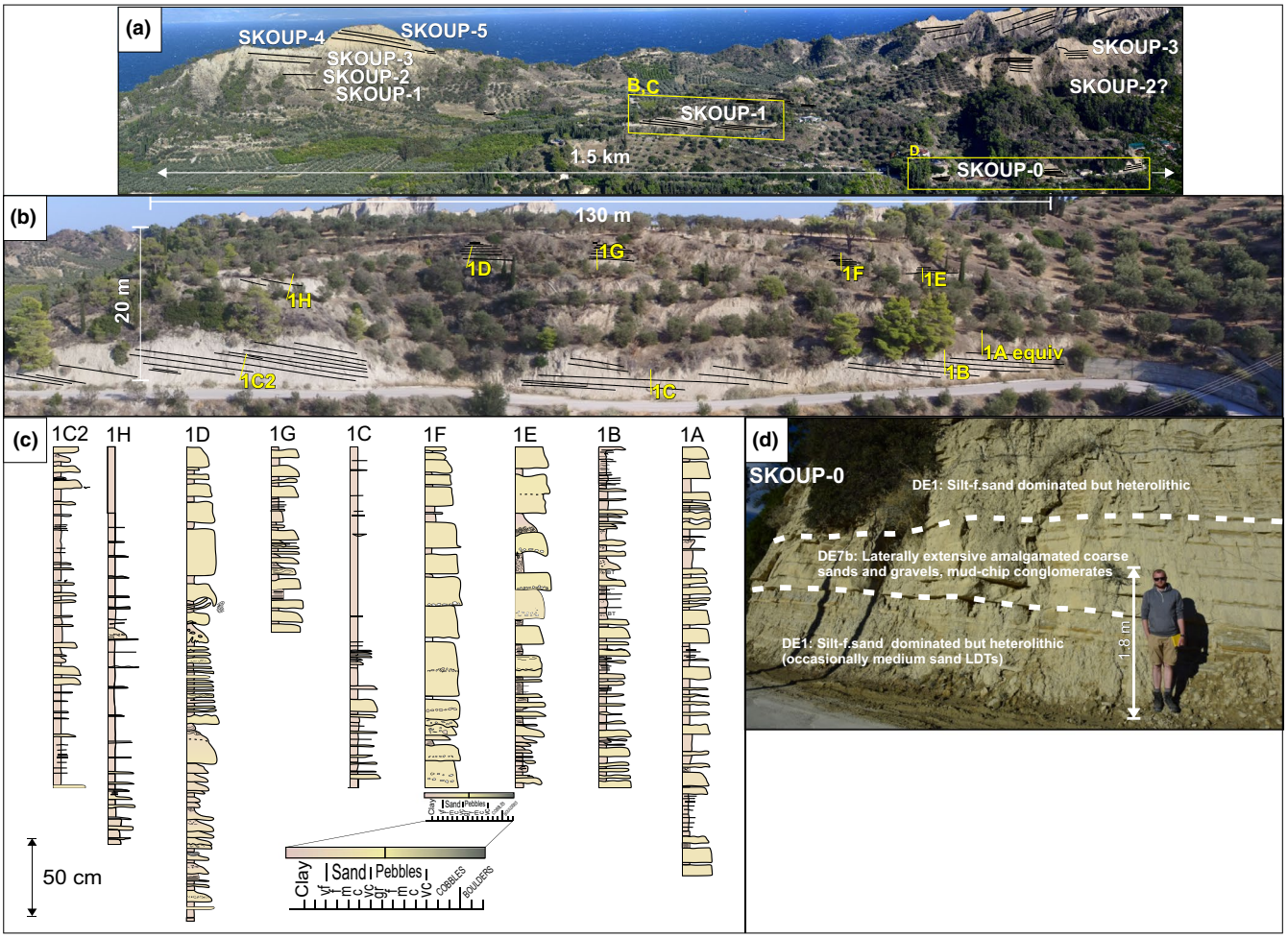

FIGURE 12 (a) Overview outlook from small cliff above western Skoupeikia looking towards the NE showing various cliff exposures with correlatable coarse-grained ridges interpreted as lobe packages. SKOUP-0 and SKOUP-1 are highlighted in yellow boxes. (b) Overview of SKOUP-1 exposures in a terraced olive grove with log localities presented in C highlighted in yellow. (c) Sedimentary logs from SKOUP-1 exposures shown in B highlighted the generally finer grained facies compared to proximal deposits and development of typical lobe facies. No correlation is implied. (d) Outcrop photograph in SKOUP-0 showing tabular, amalgamated sandstones overlying interbedded siltstones and mudstones (DE7b and DE1) similar to lobe element deposits described in MacDonald et al. (2011)

and metamorphic clasts, indicating connection to the same hinterland drainage as the Evrostini/Ilias delta. The proximal part of the Pyrgos Member is at the junction of the Ilias delta and the evolving WXF segment.

The Pyrgos Member is considered part of the broader Ilias delta system; however, we propose it as a distinct mappable unit based on extensive exposures of conglomeratic channel-fills (DE4), which is markedly different to stratigraphy adjacent and beneath it. This downdip continuity has not been recognised in previous mapping (e.g. Rohais, Eschard, et al., 2007) as this was focussed to the west of the West Xylokastro Fault. The Pyrgos Member may be stratigraphically equivalent to WX8 as it erodes into WX7, however poor outcrop continuity and an absence of biostratigraphic constraint across the Skoupeikos River valley does not permit a direct observable connection over a broad area of no exposure, and so they are considered and described separately. We acknowledge that the Pyrgos Member channel-fills may well have been a feeder system for WX8.

4.3.10 | Fault-proximal RDF (Western Transverse System and Central Transverse System)

In the western Skoupeikos River valley (Figures 2 and 13b), stratigraphy 0–1.5 km from the fault scarp is exposed. These comprise basinward (northward) dipping marlstones and sandstones as part of a fault related monocline (Lewis, Jackson, & Gawthorpe, 2015; Sharp et al., 2000) equivalent to the lowest stratigraphy in the area (WX1 and WX2). These are interdigitated with chaotic, large boulder clast breccias and conglomerates and only reach ~500 m away from the fault (Figure 13c). We interpret these as tallus deposits comprising rockfall breccias and mass wasting events related to

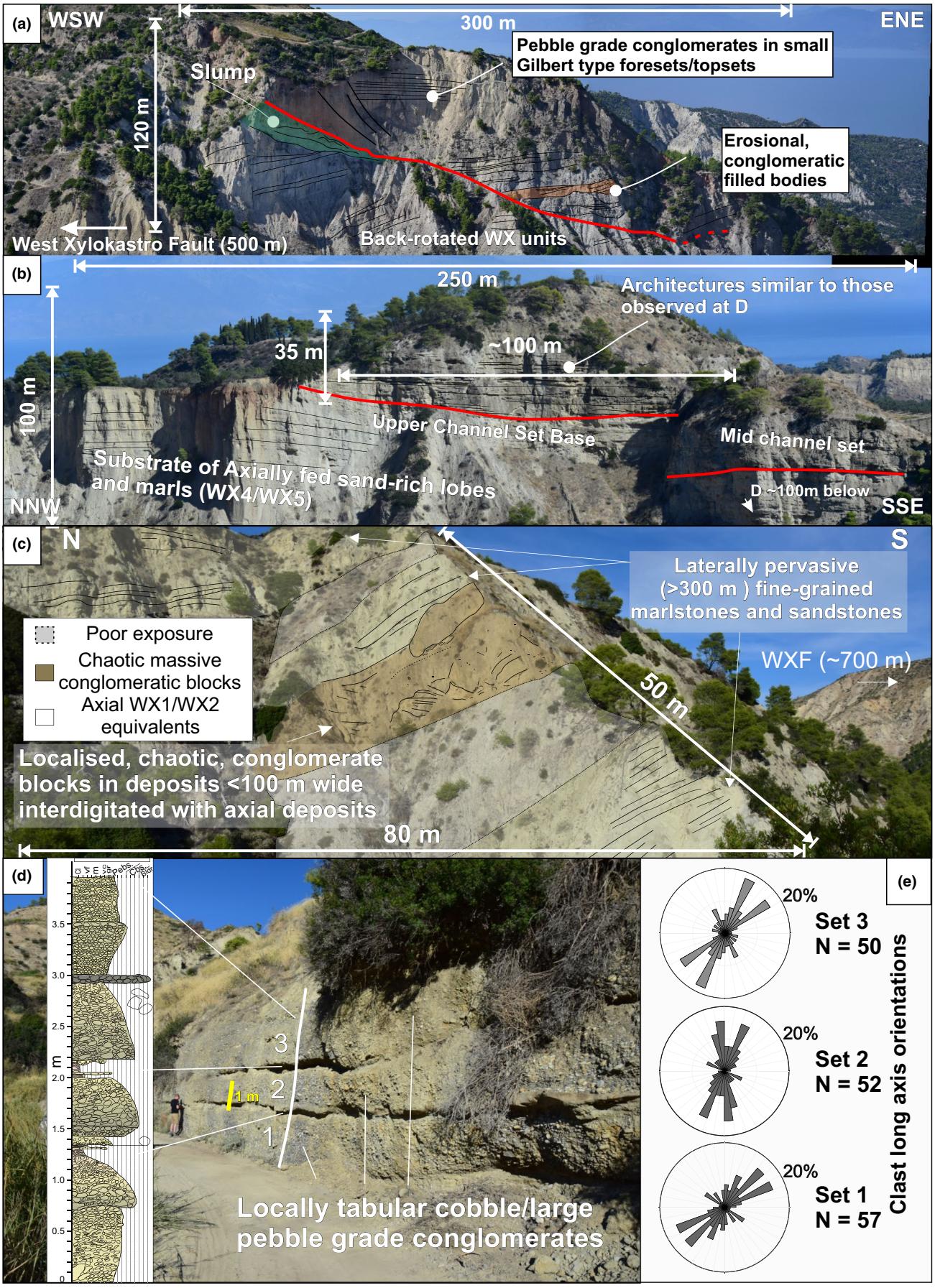
(a)
WSW
ENE
300 m
120 m
Slump
Pebble grade conglomerates in small Gilbert type foresets/topsets
Erosional, conglomeratic filled bodies
West Xylokastro Fault (500 m)
Back-rotated WX units
(b)
250 m
100 m
35 m
~100 m
Architectures similar to those observed at D
Upper Channel Set Base
Mid channel set
Substrate of Axially fed sand-rich lobes and marls (WX4/WX5)
D ~100m below
NNW
SSE
(c)
N
S
Laterally pervasive (>300 m) fine-grained marlstones and sandstones
Poor exposure
Chaotic massive conglomeratic blocks
Axial WX1/WX2 equivalents
WXF (~700 m)
50 m
Localised, chaotic, conglomerate blocks in deposits <100 m wide interdigitated with axial deposits
80 m
(d)
m
3.5
3.0
2.5
2.0
1.5
1.0
0.5
0
3
2
1
1 m
Locally tabular cobble/large pebble grade conglomerates
(e)
20%
Set 3
N = 50
20%
Set 2
N = 52
20%
Set 1
N = 57
Clast long axis orientations

FIGURE 13 (a) Overview of the proximal portion of the Pyrgos Member uncomformably overlying and incising into axial WX deposits, taken from northern slope of the West Xylokastro Horst. (b) Pyrgos member channel forms near Skoupeikia with accessible, similar architectures observed in (d) at the base of the cliff. (c) Outcrop photograph in the lower Skoupeikos valley showing chaotic, rock fall deposits forming a significant angular unconformity on seaward/basinward tilted axial WX1/2 deposits. (d) Conglomeratic deposits typical of the Pyrgos Member. (e) Pebble long-axis orientations measured in (d). These have not been restored for any tectonic tilt in the absence of a definitive palaeohorizontal; however bedding is approximately horizontal in this location

fault scarp degradation or input from minor, transverse, proximal point sources on the uplifting Xylokastro Horst.

Toward the centre of the fault, the characteristics of the hangingwall transverse fairway are notably different from that in the west (Pyrgos Member and WTS). The hangingwall apron is more mud-rich and mass-transport dominated, with thinner, less extensive (1–15 m thick, 100–500 m wide) mass transport deposits (debris flows, slumps, slides) interbedded with the axial fairway toward the east. To the west we observe the development of large, mass transport complexes (e.g. Likoporiá Slide) and chaotic mudstone-rich stratigraphy onlapped by undifferentiated, axially derived sand-rich stratigraphy (Figures 2, 3b and 14).

4.3.11 | Likoporiá Slide

The Likoporiá Slide covers ~4 km^2, with 50–100 m thick thrust sheets and ~300 m high sheath folds in the northern portion (Figure 14). Thrusts and folds verge N/NE, in keeping with transport from the WXF scarp-apron into the main depocentre. The Likoporiá Slide is mud-dominated, with deformation picked out by sandstone and conglomeratic beds, which highlight ~100 m amplitude, tight recumbent folds and thrust faults (Figure 14b,c). Conglomerates show an absence of metamorphic clasts, suggesting that the Likoporiá Slide was sourced from the WXF scarp. The thrust sheets at the toe of the Likoporiá slide extend 2.5 km from the hangingwall cut-off indicating that the basinward (northern) extent of the central transverse fairway/Likoporiá Slide is much greater than in the east. With the exception of the thrusted toe of the Likoporiá Slide (Figure 14a), the northern part of the Likoporiá Slide is offset by an intra-basinal fault (Minor Fault 3, Figure 14c), the hangingwall of which hosts the Upper WX succession. Several correlative horizons (Numbered 10–45) are present within Upper WX. The position of the Likoporiá Slide within the footwall of Minor Fault 3 means it must pre-date WX8. However the western edge of the Likoporiá slide is poorly exposed and so accurate determination of its timing carries some uncertainty.

5 | BASIN EVOLUTION OF THE WXFB

5.1 | Lower WX

Figure 15 summarises our interpretation of the co-evolution of structural and depositional elements and their ultimate impact on the palaeogeography of the WXFB. WX1 records Ilias fan delta progradation over the western tip of the WXF, and the initial infill of the depocentre with >30 m of fine-grained material in the distal parts of the basin (e.g. Figure 15a, Panel E in Figures 8b and 9). Coarser material was restricted to the proximal bottomsets (i.e. thin conglomerates of upper WX1 in Figure 6d,e). At the base of foresets, Surface 2 comprises a composite scoured surface with coarse clastic sediments overlying Surface 2 in the deeper basin (panel F in Figure 9), suggesting a sediment bypass-zone (Elliot, 2000; Stevenson et al., 2015). Comparatively low throw (<50 m) and sub-parallel intra-basinal faults affected parts of the axial fairway, focussing conglomeratic hyperconcentrated/debris flows into subsidiary depocentres in the hangingwall of minor faults, whereas finer grained turbidity currents could deposit across the depocentre, even on intra-basinal highs.

In the proximal bottomset, Surface 3 hosts chutes and small channels (Figures 6a,c and 15b), whilst Surface 3 is overlain distally by ~5 m fine-grained interval between conglomeratic material of WX2 and WX3 near Stomio (Figure 9a) and comprises a compensational surface at the lateral and distal fringe of WX2 near Skoupeikia/Kalithea (Figure 8b). Due to the widespread increase in sediment supply to the deep-water, we interpret the formation of Surface 3 to be related to a relative base level fall (Figure S2), followed by progradation of the delta. The Stomio faces record a change from axial to fringe position, which may be related to changes in sediment dispersal during the relative base level fall or by realignment of the updip sediment pathway with intra-basinal minor faults that routed sediment elsewhere. This change in dispersal pattern results in downdip locations receiving less coarse-grained supply and an increase in mass transport deposits (DE9) from the WX2 and WX3 units despite the interpreted relative base-level fall. MTDs in the modern, offshore Gulf tend to be in-phase with local increased sediment supply patterns providing a pre-conditioning mechanism for slope failure (Beckers et al., 2018). In the WXFB, exposure of parts of the uplifting WXF footwall and apron during the interpreted relative base level fall might have provided increased supply permitting such pre-conditioning.

WX4 mudstones and marlstones highlight a basin-wide hiatus of coarse clastic deposition. Correlation of WX4 into the Ilias fan delta with a transgressive surface and associated

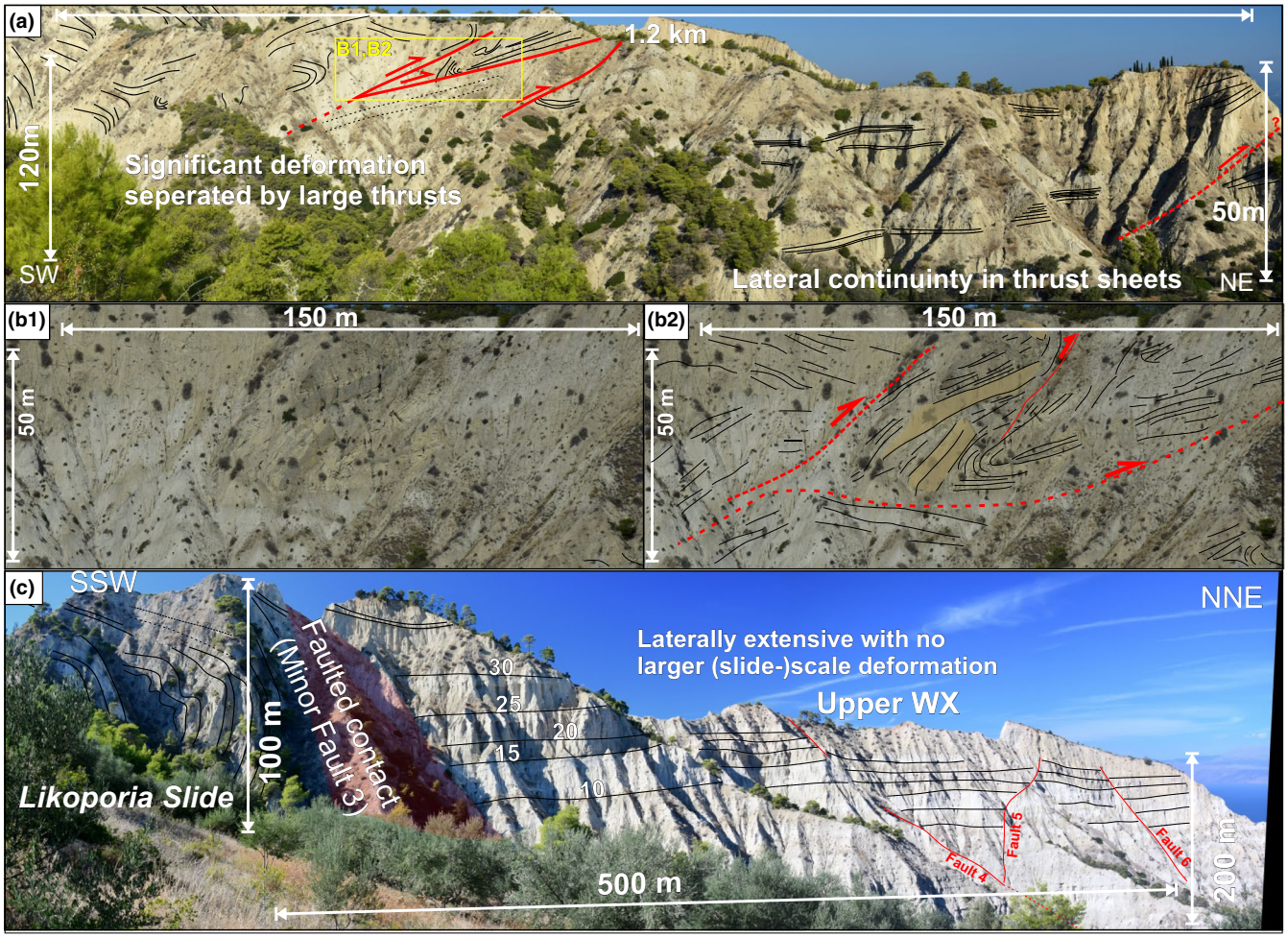

FIGURE 14 The north-eastern toe of the Likoporiá Slide is dominated by several thrust sheets showing overturned soft-sediment fault-propagation folds, with its southern-most portion comprising an extensive sheath fold. (a) Thrust faults (and associated folds) verge northwards indicative of a northward transport direction. (b) Deformation in the slide can intensely deform the stratigraphy, overturning or rotating of bedding and displacement along intra-slide thrusts. Folds have wavelengths and amplitudes varying from 50 to 100 m. (c) The Likoporia Slide (left) has a large (>100 m) amplitude sheath fold in it's central portion which is in the immediate footwall of minor fault 3 which hosts the Upper WX stratigraphy correlated from the west. This Upper WX stratigraphy is dissected by minor faults (throws between 10 and 40 m)

relative highstand portion of the fan delta, WX5, which marks the return of coarse clastic sediment supply to the deep-water basin (Figure 15C) shown by the downlap of WX5 foresets onto WX4 (Figure 10). The distal WX4 contains slumps suggesting the maintenance of transverse supply. Whilst distinct to WX4, we propose that the Likoporiá Slide was contemporaneous as there appears to be little influence on WX2-3 stratigraphy compared to the northward palaeocurrent swing noted in the overlying WX6 (Figure 9). However, the precise timing of the Likoporia Slide remains uncertain. Base level rise as a trigger for mass-transport emplacement is well documented in similar systems (e.g. Beckers et al., 2018; Zitter et al., 2012), although discriminating this from other allogenic triggers is challenging.

WX6 is marked by debrites and sand-rich turbidite channel-fills. We interpret this lateral variation to reflect the respective positions relative to the axis of the delta through time; off-axis conglomeratic lenses (bars) in the western part of the delta, compared to channel-fills produced by highly erosive flows downdip of principal fluvial outputs (Figure 15d). Surface 6/WX6 could represent another relative base-level fall. However, this cannot be confirmed by updip erosive surfaces (unlike in WX3) and so could represent localised changes in sediment dispersal patterns, or both. Intra-WX6 architectural features, such as Surface 6.2, which thins and onlaps onto the foresets, are interpreted to be a result of higher-order sediment flux fluctuations, or 'noise' within the base-level change signal (Jerolmack & Paola, 2010), or reflect local, autogenic changes typical of bottomset architectures. Downdip, WX6 shows alternation at metre scales from conglomerate-dominated packages to finer grained packages containing slumps and cohesive debrites (e.g. fine-grained interval at the base of WX6 overlain by conglomeratic and sand-rich

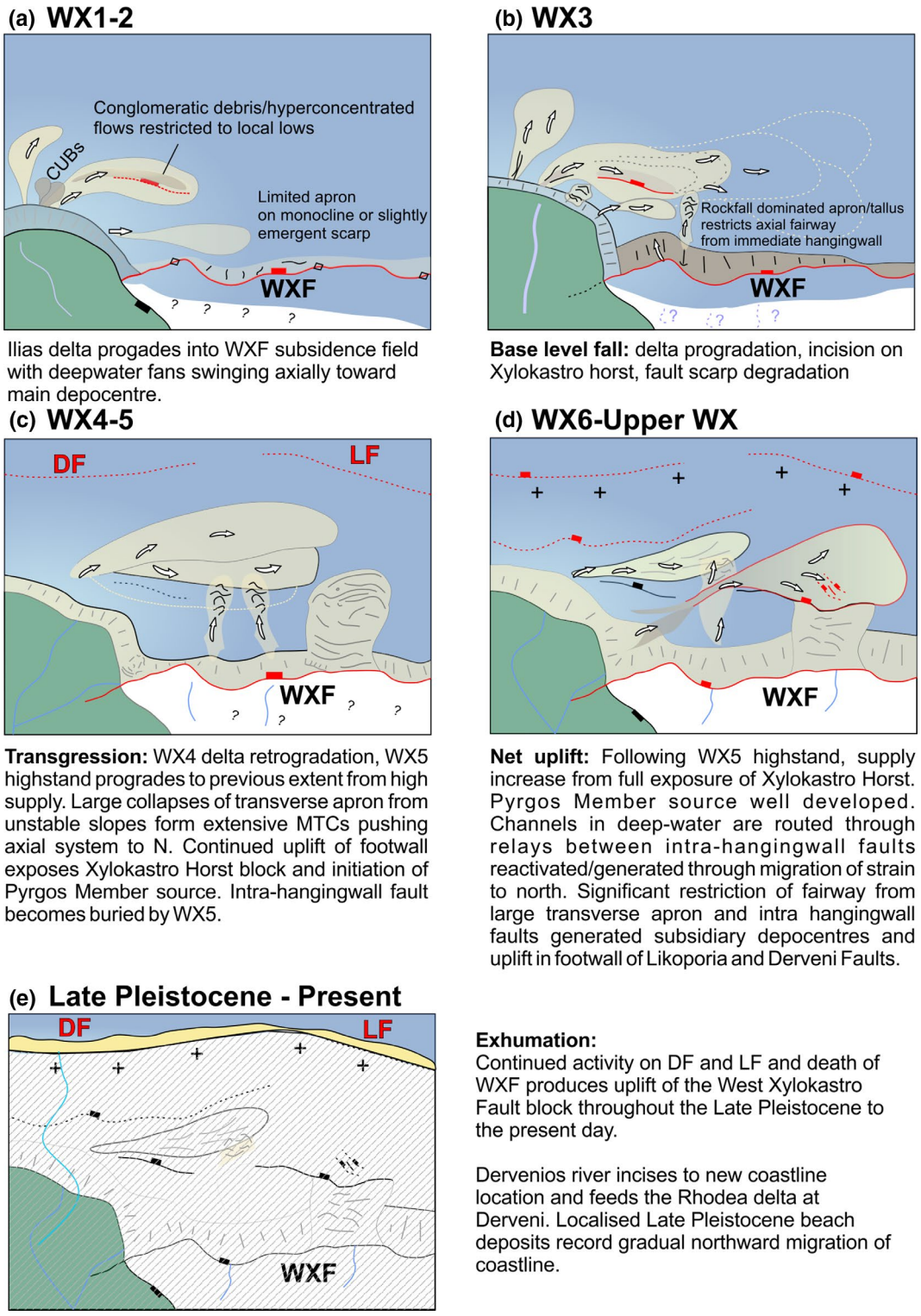

FIGURE 15 Summary evolutionary cartoons for the development of the WXFB hangingwall. (WXF = WXF, DF = Derveni Fault, LF = Offshore Likoporiá Fault)

sheets in Figures 8b and 9). WX7, WX8 and the Pyrgos Member mark continued progradation and supply of this deep-water system, which reaches farther out to the east as sand-rich lobe deposits (Figure 15d). The broadening out of the depocentre in this region may have promoted these lobe deposits, picked out by the ~1.5 km continuous sandstone ridges south of Likoporiá within WX8 (e.g. Figure 12a). However, variable palaeocurrent orientations (e.g. Figure 9) may indicate significant local variation and/or confinement from intra-basinal structures (Ge, Nemec,

Gawthorpe, & Hansen, 2017; Ge, Nemec, Gawthorpe, Rotevatn, & Hansen, 2018). These show focussing within the broad depositional low into the hangingwall of Minor Fault 3. The exact position and orientations of these lobate deposits is uncertain given the poor accessibility and more heavily vegetated exposures in this region. Upper WX represents the last deep-water stratigraphy seen in the area prior to uplift to the present day configuration (Figure 15e).

5.2 | Comparison with previous studies

The recent erosion and lack of exposure of the upper part of the foreset and topset (if present) in the Ilias exposures makes definitive determination of base-level changes uncertain, and so has given rise to a number of models (Gobo, Ghinassi, & Nemec, 2014; Gobo, Ghinassi, Nemec, Sjursen, 2014; Rohais et al., 2008; Rubi et al., 2018; Zhong et al., 2018). The primary focus of previous studies has been on higher-order variability and sedimentary processes within the immediate bottomset of WX4, WX5 and WX6 in the broader stratigraphic scheme. Nevertheless, interpretations made on the broader evolution have a number of agreements and inconsistencies with the interpretation presented here. The expansion of area studied both spatially and stratigraphically presented here compared to previous studies provides greater context for the Ilias delta. For example, Rohais et al. (2008) place no significance on Surface 4 despite observing the truncations, and subsequent backstepping of the delta, which we interpret as the onset of a regional transgression. Instead, Rohais et al. (2008) attribute this transgression to a much thinner sand-rich stratigraphy between Surface 4.2 and Surface 5 in our scheme. We fail to see how this transgression can only be limited to this portion given the truncated and downlapping relationship underneath (either side of Surface 4 in our scheme) and that the backstepping of the delta must have occurred sooner than this (i.e. during Surface 4).

These differences reflect the uncertainties in outcrop correlation, which Rubi et al. (2018) and this study have sought to address through the use of 3D outcrop models. Our interpretation of base-level change is broadly in agreement with Rubi et al. (2018), albeit minor differences exist. For example, Surface 6 base-level fall in this study and Rubi et al. (2018) is overlain in the foreset to bottomset transition by conglomeratic deposits between Surface 6 and 6.1 in our scheme (Figure 10c), which we correlate to conglomerate-rich deposits of similar thickness downdip in the bottomset. However, Rubi et al. (2018) interpret that this package onlaps the erosional surface updip within an area of no exposure and so mark this as the onset of a transgression and deposition up the foreset slope. We see no reason to invoke this, as we observe a consistently conglomerate-rich WX6 unit that thins up onto, but is largely conformable with, the foreset (Figure 10d). We only observe onlaps in the bottomset at Surface 7, which coincide updip to a fining up sequence, frequent appearance of finer grained stratigraphy, and a more consistent back stepping of the delta. Our observations of sub-unit scale fluctuations in debrite- and turbidite-dominated stratigraphy (e.g. intra WX5) are in accordance with the observations and interpretations of Gobo, Ghinassi and Nemec (2014), Gobo, Ghinassi, Nemec, and Sjursen (2014) of high-frequency changes within the base-level variability (Section 5.1). At the larger scale, Rohais and Moretti (2017) and Zhong et al. (2018) have considered the broader context of the West Xylokastro stratigraphy. We see no evidence to support the existence or influence of north-south transfer faults interpreted in Zhong et al. (2018). However, we agree that the Ilias delta and the bottomset region are dissected by a number of minor faults that likely strongly impacted depositional fairways producing a dominant eastward axial fairway (sensu. Rohais, Eschard, et al., 2007; Rohais, Joannin, et al., 2007; Rohais et al., 2008). Contrary with Rohais and Moretti (2017), we do not interpret the West Xylokastro hangingwall fill as representing a single, fault proximal, asymmetrical channel complex with a northern asymmetrical levee (sensu examples from Baja California in Kane et al., 2009) and instead interpret the system on the basis of the observations presented here, as a system chiefly comprising channelised lobes and MTDs.

6 | DISCUSSION

6.1 | The role of intrabasinal structures on deep-water syn-rift sedimentation

Intra-basinal faults (Figures 2 and 16) dissected the basin floor of the WXFB and form a key control on the distribution of depositional elements. At the local scale, intra-basinal faults can control the location of subsidiary depocentres within the fault block (e.g. Figures 15 and 16a). For example, WX8 exposures sit within the subsidiary depocentre generated by Minor Fault 3, which was active at this time (Figure 15d). This topographic variability on the basin floor can influence sediment dispersal patterns. For example, above the footwall of Minor Fault 1 the WX2/WX3 units are dominated by finer grained, sand-rich turbidites (DE5, DE7b, DE8) and comprise coarse grained facies (i.e. DE7a conglomeratic sheets) in its hangingwall indicating its control on flows during deposition. Further to the south of this structure, tabular conglomerates are present at similar stratigraphic levels. Higher concentration laminar flows, such as conglomeratic sheet-forming debris flows, are ground hugging and focussed into topographic lows, whereas dilute turbidity currents can deposit on topographic highs (Figure 16b,c). Similar topographic

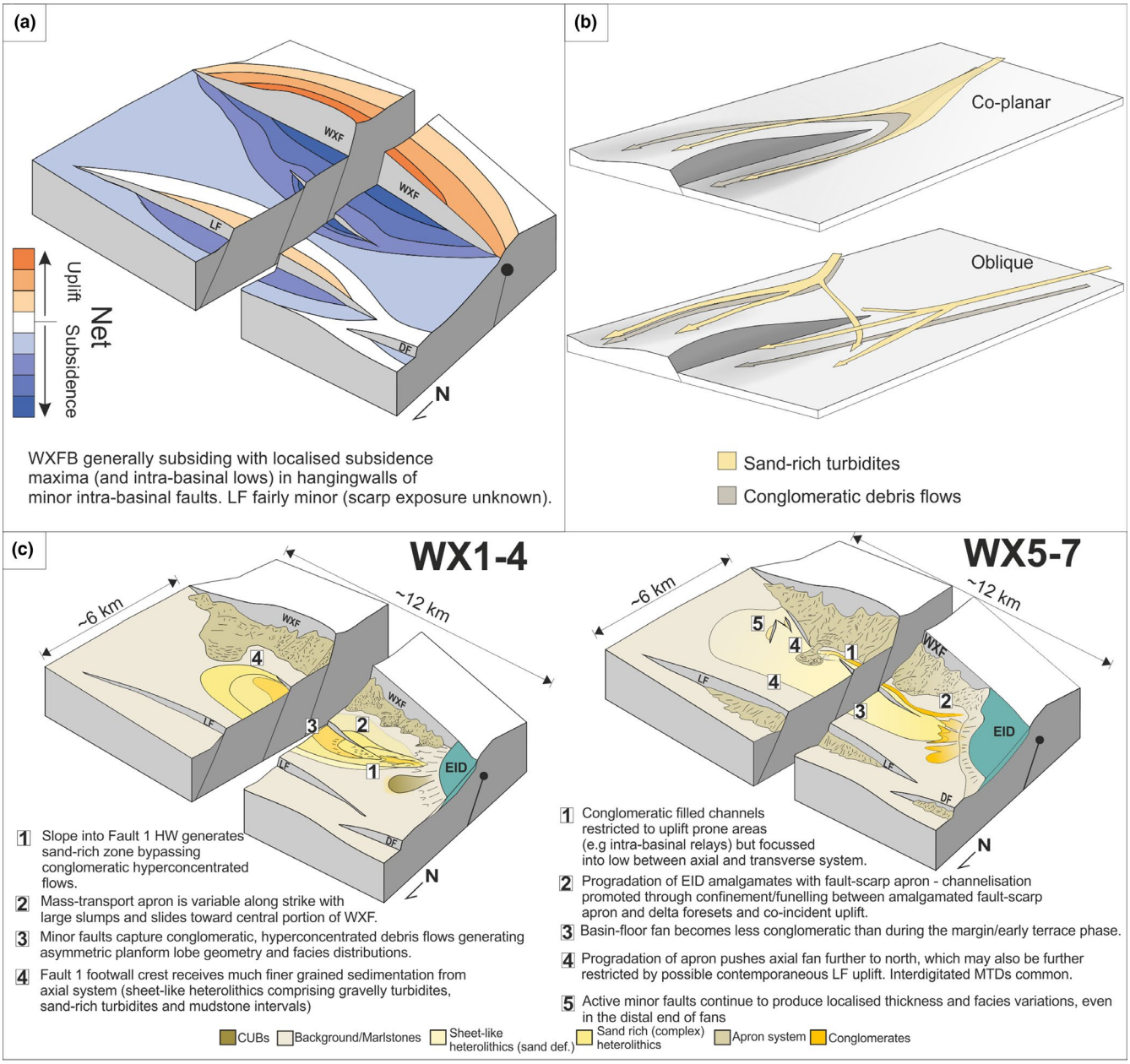

FIGURE 16 (a) Intra-basinal structures act to locally enhance or disturb the subsidence field of the West Xylokastro Fault and locally capture coarse grained depositional elements such as conglomeratic sheets (modified from Gawthorpe et al., 1994). (b) Intrabasinal structures preferentially focus certain flow types into topographic flows which may receive more or less sediment according to the obliquity of an incoming flow (modified after Bakke et al., 2013). (c) The effects of intrabasinal structures complicate the multi-input system creating fan asymmetry and disturbing typical conceptual facies tracts for lobate systems. Through the progressive evolution of the system to Upper WX times, the apron and EID merge generating highly efficient flow pathways promoting channelization between the fault scarp apron and the axial system. Intra-basinal relays influence channel pathways

effects on gravity currents have been described from outcrop (Bakke et al., 2013) and from observations in numerical models (Al Ja'Aidi, 2000; Al Ja'Aidi, McCaffrey, & Kneller, 2004; Athmer et al., 2010; Ge et al., 2017, 2018). The incidence angle of flows with respect to an intra-basinal structure also influence where the coarsest/ground-hugging flows are routed (Figures 15a,b and 16b). River avulsions on the delta or sourcing of flows along a multi-point apron may route flows away from the hangingwall of intra-basinal structures, which can explain the fluctuations between conglomerates to sand-rich stratigraphy within WX3 in the hangingwall of Minor Fault 1. Alternatively, this variation is attributable to high-order sediment supply fluctuations triggered by changes in climate and/or seasonality (Armitage, Duller, Whittaker, & Allen, 2011; Collier et al., 2000). The complexity from such a topographically

variable basin floor means it is difficult to confidently attribute a 1D (e.g. well-log) or limited 2D (e.g. isolated outcrop) expression to such variations without considering the entire lateral extent of a stratigraphic unit. Figure 16b,c highlights how these intrabasinal structures can act to impact the morphology of lobes and produce asymmetric distributions of conglomerate (i.e. Lower WX) or promote channelization in areas of pre-existing confinement (e.g. in the syncline developed between the hangingwall apron and the footwall dip-slope of Minor Fault 1). This proximity of channels to the immediate hangingwall is observed in similar systems attributed to hangingwall monoclines/synclines (Kane, Catterall, McCaffrey, & Martinsen, 2010; Kane et al., 2009). The confinement could be generated by a combination of fault-related topography and the topography of a transverse apron.

6.2 | Controls on the formation and styles of key stratal surfaces and intervals

In the absence of biostratigraphy or tephrostratigraphy, key stratal surfaces and intervals can aid correlation. WX4 provides a mudstone-rich 10–30 m thick interval that is traceable throughout the study area. In the Ilias fan delta, WX4 is defined by finer grained deposits, with a geometry indicative of transgression of the delta (Figure 10). Given its extent, we interpret WX4 to represent a basin-wide hiatus of sedimentation, rather than localised or restricted avulsions on the Ilias fan delta, although comparative exposure of deep-water stratigraphy to the west of the delta is limited. WX4 is interpreted to have formed during a relative base-level rise, although a decrease in hinterland sediment supply due to climatic or drainage variation cannot be ruled out. Such intervals are common in deep-water syn-rift successions and attributed to phases of fault activity and associated deepening. However distinguishing these from eustatic base-level rise alone is challenging without robust chronostratigraphy (Dorsey, Umhoefer, & Falk, 1997; Henstra et al., 2016; Strachan et al., 2013; Young, Gawthorpe, & Sharp, 2002). The WX4 transgression was outpaced during the following highstand by progradation of WX5 in the Ilias fan delta that returned coarse-grained material to the most distal part of the West Xylokastro system.

Regressive surfaces (formed by base-level fall and/or increased sediment supply) are most apparent and confidently traced in the foresets and proximal bottomset, where they are associated with geometric relationships, lithofacies changes, and architectural changes. However, even within the proximal bottomsets, regressive surfaces show substantial variability over 1–2 km^2. The variability described over ~500 m in Surface 2 from a composite bypass surface with lithological similarity to the basal surface of conglomeratic CUBs highlights how identification of such surfaces in 1D data may prove elusive. The change in character of Surface 2 could be attributed to diachroneity/time of formation through a given supply cycle forming such a surface (Barrett, Hodgson, Collier, & Dorrell, 2018; Hodgson, Kane, Flint, Brunt, & Ortiz-Karpf, 2016), or may reflect lateral variability in the dominant process and nature of bypass operating in the highly variable bottomset (Stevenson et al., 2015).

Regressive surfaces can be more subtle downdip. Surface 3 (WX2-WX3 boundary) in the proximal bottomsets and Ilias fan delta is deeply (~10–35 m) erosive, hosting conglomeratic chute-fills. However, downdip, near Stomio (Figures 2 and 8a), in the hangingwall of Minor Fault 1, Surface 3 is relatively conformable above WX2 conglomeratic sheets, and overlain by a 3–5 m finer grained interval (basal WX3) before returning to conglomerate-rich sheets and lenticular heterolithics. The pervasive erosive nature of this surface in the proximal region is difficult to reconcile with the fine-grained interval overlying Surface 3 in the Stomio region, representing a temporary starvation of sediment to the Minor Fault 1 hangingwall. To the south, at the eastern edge of the footwall dip slope of Minor Fault 1, are tabular WX3 conglomerates (Figure 13d). This temporary starvation and change in character from the proximal expression of Surface 3 in the hangingwall of Minor Fault 1 represents a lateral/off-axis deep-water expression of Surface 3. Such lateral changes may be produced or enhanced by the complexity of the sediment fairway where complex basin-floor topography from intra-basinal structures (Section 6.1) and/or mass-transport deposits (Section 6.3) cause rerouting of flows. Complex fairway topography promotes the possibilities of ponding, sediment storage or non-deposition along the depositional pathway which can 'shred', enhance or dampen updip stratigraphic signals (Forzoni, Storms, Whittaker, & Jager, 2014; Jerolmack & Paola, 2010). This leads to stratigraphic surfaces that may exhibit characters atypical of the causal, regional allogenic mechanism or event (e.g. mudstones during a base-level fall/supply increase) to which they correlate because of greater in-situ control.

Subsidence and supply variation along a given fault segment can produce notably different stratigraphic architectures and responses (Barrett et al., 2019, 2018; Gawthorpe et al., 1994). The applicability of this in axial deep-water systems is complicated, where deposits are a product of in-situ allogenic parameters (i.e. high, fault centre subsidence) but strongly rely on transport and reworking of material from locations updip (i.e. fault-tip deltas with lower subsidence and high sensitivities to eustasy). The representation of stratigraphic surfaces in linked, syn-rift deep-water systems may therefore lie in whether the system is accommodation (in-situ) or supply (Gilbert-delta) dominated at a given time or location (Burgess & Hovius, 1998; Carvajal & Steel, 2006; Zhang, Burgess, Granjeon, & Steel, 2019; Zhang, Kim, Olariu, & Steel, 2019). Zhang, Burgess, et al. (2019) and Zhang, Kim, et al. (2019) infer that this is principally reliant on shelf width

and amplitude of base-level change from numerical models, where high amplitudes of base-level variation decrease deep-water sediment export only in large shelf width, supply-dominated systems. However, Zhang et al. (2019) focus on wide, well-established shelves. Syn-rift systems exhibit both very high rates and magnitudes of accommodation generation and high supply due to young, steep drainages from rapidly uplifting hinterlands. This further acts to promote narrow shelves, despite high sediment supply providing continued export of sediment to the deep-water realm (e.g. Strachan et al., 2013). We observe that the most limited delivery of coarse material to the deep-water realm was during transgressions (e.g. WX4). These periods may reflect the only time at which the system was truly accommodation-dominated. The restriction of this phenomenon to WX4, highlights that the *rate* rather than magnitude of relative base-level change may be a key control on the delivery of coarse grained sediment to deep-water rift settings such as the WXFB. Shut-downs of coarse-grained supply in such systems may be temporally restricted (e.g. during transgressions) or permanent and trigger the abandonment of a system. For example, longer-term changes in delta position (sensu. Rohais et al., 2008) or drainage reversal according to catchment evolution could end delivery to the deep-water.

6.3 | Interaction of multiple systems in deep-water rift basins and their effect on stratigraphic architecture

The WXFB was fed by both an axial deltaic and localised, transverse fault-scarp apron. Extensive mass-transport deposits coeval with much of the Lower WX dominate the central part of the transverse system. Slumps and debrites up to ~2–3 km from the fault scarp have limited lateral extents and thicknesses (typically <500 m wide and <10 m thick), whereas very large, multi-kilometric slides (e.g. Likoporiá Slide) have a >2 km extent into the basin. Minor and intermediate slumps appear to have longer run-out distances and can interdigitate with axial stratigraphy. These produce bed-scale undulations of seabed topography (e.g. slumps underlying winged conglomerates; Figure 7), which are mantled by overlying axial deposits. However, the apron itself imparts a greater control on the entire axial system, forcing it northwards. Conceptual models of rift basins and single input numerical models predict that deep-water flows will preferentially flow towards and deposit in fault central areas (Athmer et al., 2010; Gawthorpe & Leeder, 2000; Ge et al., 2017, 2018; Haughton et al., 2009; Jackson et al., 2012). Jackson et al. (2012) proposed forelimbs of fault-related monoclines may offset axial deep-water systems from being proximal to a fault, with surface breaking faults allowing axial systems to run parallel to and deposit in the immediate hangingwall to a fault. Similarly, where a transverse input is also operating, we observe that this acts to offset the axial system from the fault scarp. The most noteable expression of this is the Likoporiá Slide, which imparted at least 3 km of northward shift to the axial system. Recognizing transverse systems and their possible impact on sediment routing within axial systems becomes important in subsurface applications; but may be difficult where transverse systems are small, steep and chaotic, and consequently poorly imaged.

This interaction creates a 'Zone of Fairway Restriction' ('ZFR' - Figure 17a). Whilst early fault growth (Figure 17 a(A), b(B)) does not produce a large scarp, instabilities on the front of a monocline can trigger large, rotational slides forcing axial systems substantially outboard of the fault location. Local denudation of the structural high may occur where relative base-level fall results in sub-aerial exposure (Figure 17 a(B), a(D), and a(F)). If the scarp is emergent and fed by an extensive and exposed margin, the transverse system may be well-developed and force the axial fairway substantially up the hangingwall dipslope uptowards the footwall crest of the next basinward fault or further into an open margin (Figure 17-a(E)). High supply transverse systems may be able to fill their immediate hangingwalls permitting development of narrow littoral zones/shorelines atop aprons. If supply is high and constant enough, Gilbert-type deltas, may even form at fault centres, for example, Brae systems of the South Viking Graben (Turner & Allen, 1991; Turner, Bastidas, et al., 2018; Turner, Cronin, et al., 2018), modern and Pleistocene western Gulf of Corinth (Dart, Collier, Gawthorpe, Keller, & Nichols, 1994; Ford et al., 2007; Backert, Ford, & Malartre, 2010; Ford et al., 2016; Beckers et al., 2018). Conversely, if a drainage reversal to the transverse system were to occur, this could lead to a decrease in axial fairway restriction, with no (or limited) drainage contribution to the transverse fairway.

Figure 17a highlights a continuum of scenarios that could be present in space along a fault segment (e.g. Hodgson & Haughton, 2004) or through the progressive evolution of a fault block. Figure 17b shows an approximate temporal evolution where a monocline-driven mass transport dominated apron can initially dominate the immediate hangingwall followed by footwall degradation, which may be pulsed due to periods of quiescence and/or eustatic base-level fluctuation.

Mixed input systems may experience different responses to allogenic controls (sediment supply, seismicity, eustatic sea-level variation, and structural topography), and may operate in- or out-of-phase. Fault-scarp apron supply has been linked to fault activity, with accommodation increase accompanied by chaotic degradation of fault scarps and sedimentation (Henstra et al., 2016; Leppard & Gawthorpe, 2006; Strachan et al., 2013). Fault activity and subsidence may lead to relative base-level increases throughout the hangingwall, including fault tip deltas (Barrett et al., 2019; Collier

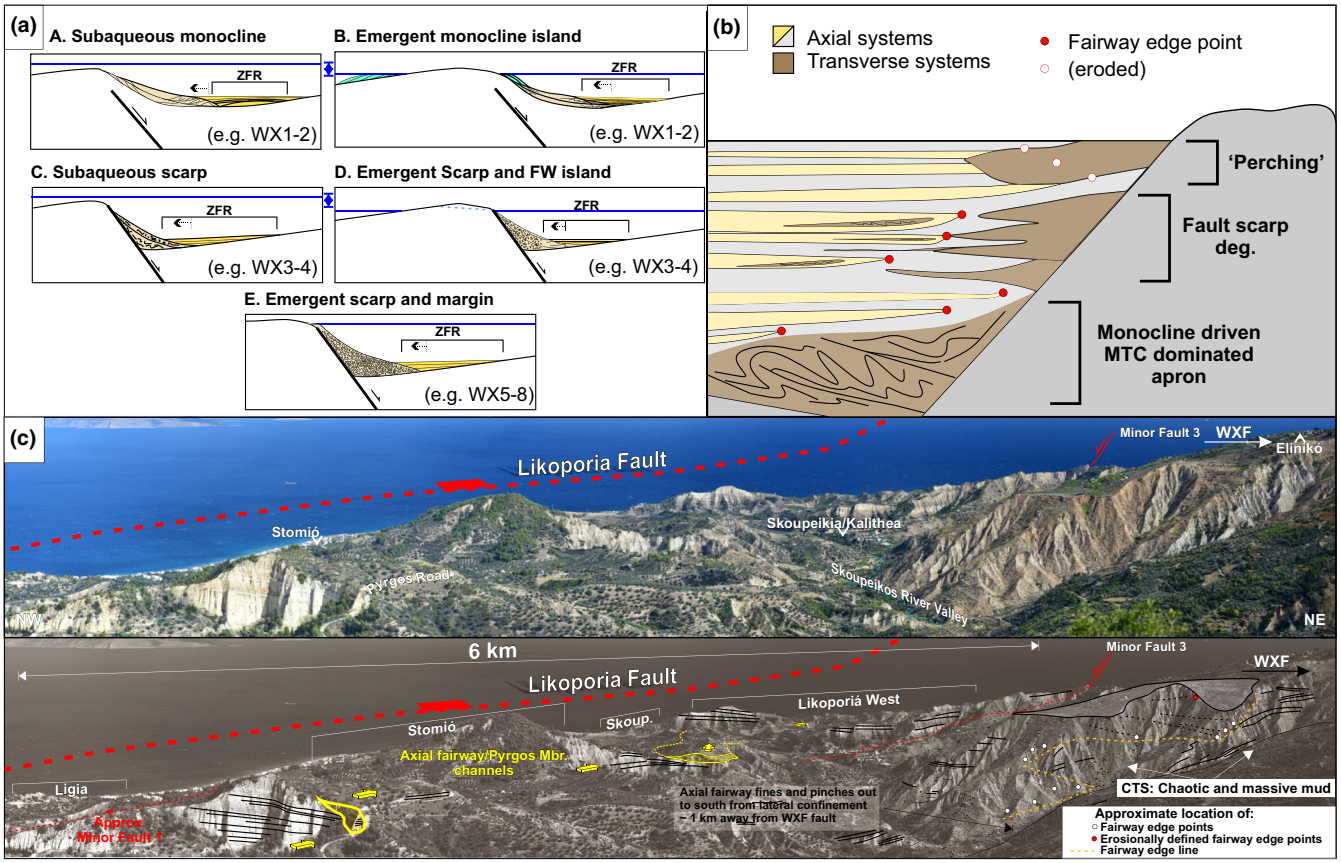

FIGURE 17 (a) Endmember models for mixed-input deep-water syn-rift deposition in half-graben settings. ZFR = Zone of fairway restriction, with arrow showing expansion resulting from filling of space by axial system at a rate greater than sedimentation in the transverse system. (b) Example temporal model for half-grabens transitioning from rift border margin setting to fault terrace settings. (c) Summary viewpoint from Pyrgos Hill into the West Xylokastro Fault Block highlighting the extent of the axial system and interaction with the more limited transverse system and styles of interaction seen in 17a,b.

& Gawthorpe, 1995; Gawthorpe & Leeder, 2000). However, Gilbert-type fan deltas are observed to retrograde, decreasing axial supply to the deep-water, whereas transverse systems may show increased occurrence of slumps and debrites (e.g. WX4 and Likoporiá Slide). Mass movement from steep, fault scarp slopes largely relies on pre-conditioning of slopes for failure by processes that include relative base level change, but also rapid increases in sediment supply, or drainage rearrangement (Beckers et al., 2018). In the WXFB, the size, spatial extent and stratigraphic frequency of MTDs all increase with proximity to the centre of the fault segment. Minor slumps and mass transport deposits (DE9) also become more common and thicker to the eastern end of the Stomio cliffs and in the transition to the basin floor in this part of the stratigraphy. This is consistent with being derived from an apron that would be larger and prone to over-steepening through loading and greater hydrostatic pore pressures promoting slope failures (especially during transgressions (Beckers et al., 2018)). Slumps and mass transport deposits that form the transverse apron are commonly observed in association with axial conglomeratic sheets, or sand-rich deposits (WX3 and WX6 in Figures 8 and 9) during coarse-grained delivery to the deep-water basin (Figure 9). In the western Gulf of Corinth, recent (Holocene) MTDs are spatially associated with some of the largest fan deltas (Selinous, Meganitis, Erineous) fed by the higher supply drainages in that region (Beckers et al., 2018; Ford et al., 2016; McNeil et al., 2007). Consequently, as with many MTDs, interpretation of their individual triggers is problematic making higher order temporal variation of transverse, fault-scarp aprons difficult to predict or invert. However, spatial domains that are more likely to experience frequent combinations of triggers (i.e. fault centres) are likely to be regions where the greatest impact of the transverse apron upon axial fairways is experienced.

Given the interplay of multiple systems in variable rift depocentres, it is unreasonable to expect all half-grabens to behave similarly (e.g. Prosser, 1993), even if one of many controls on stratigraphic architecture is the same across different sub-basins or input systems (e.g. eustasy). Local or restricted variations in supply and structural evolution produce both subtle and major changes in stratigraphic architecture. The intrinsic variability of these basins brings uncertainty in interpretation of isolated observations (e.g. 1D well logs) and highlights the need for integration of robust chronostratigraphy, and where

possible, linking of disconnected architectures/sub-basins. Whilst key stratal surfaces and intervals can provide correlative units, the aforementioned variability of these seen in the WXFB highlights the potential difficulties and miscorrelation in stratigraphic prediction in mixed deep-water syn-rift systems with sparse datasets (e.g. subsurface). The coarse-grained character of the WXFB provides an outcrop analogue that contrasts with typical fining-up abandonment models for deep-water syn-rift systems (e.g. Prosser, 1993; Ravnås & Steel, 1998) and confirms the need to consider, where possible, the entire evolution of various allogenic influences upon a given system.

7 | CONCLUSIONS

Detailed structural and stratigraphic mapping for the first time links Ilias delta deposits to a distal deep-water fan in the WXFB. Extensive mudstones provide key stratigraphic markers in the stratigraphy, which are related to basin-wide reduction in coarse clastic delivery in response to relative base level rise. The stratigraphic framework generated permits the variability in stratigraphic architecture and sedimentary processes to be placed in context, and the impact of allogenic and autogenic changes in the WXFB deep-water system to be considered. The WXFB is a rare example of an exhumed syn-rift deep-water depositional system that comprises coeval transverse and axial supply systems. The axial system, derived from the Evrostini/Ilias Gilbert-type fan delta, shows significant architectural variability in its proximal regions with the formation of conglomeratic chutes, lenses, sheets and convex-up bodies (CUBs) interspersed with finer grained turbidites of either lenticular or sheet-like morphologies. The transverse system is largely dominated by variably extensive slumps and slides, which significantly restrict or divert the axial system away from the immediate hangingwall, contrary to conceptual models for single-input axial turbidite systems.

The presence and character of key surfaces and intervals are complicated by structurally controlled facies distributions within the basin floor and distal bottomset, focussing conglomerate-rich flows into localised lows, with finer grained sand-rich turbidites and mudstones on localised highs. The interplay between intra-basinal structures, allogenic changes (e.g. eustasy, sediment supply) and contemporaneous input systems result in complicated stratigraphic successions at a range of temporal and spatial scales. The WXFB highlights the need to examine deep-water rift-systems, where possible, in the context of their own evolution as existing simple conceptual models over-emphasise a dominant fining upward, mudstone-rich motif. The interplay of structural and drainage evolution, depositional processes, and base-level change all show substantial spatial and temporal variability in deep-water rift settings. The complexity, reflecting multiple input points, dynamic seabed topography, and restricted, high sediment supply systems, emphasizes the requirement for models that consider all the factors influencing the variability of the basin fill.

ACKNOWLEDGEMENTS

This publication forms part of the first author's PhD project, which is funded by the Syn-Rift Systems (PETROMAKS 2) project funded by the Research Council of Norway (Project number 255229/E30) and industry partners Aker BP, ConocoPhillips, DNO, Equinor, Tullow Oil, Neptune and by the University of Leeds. TMC also thanks Haralambos Kranis, Martin Muravchik, Gijs Henstra, Gauti Eliassen, Charlotte Allen and Jamie Ranaldi for their assistance and discussions in and out of the field. Stereonet plots were generated in Stereonet10, a free software from Rick Allmendinger and can be downloaded at www.geo.cornell.edu/geology/faculty/RWA/. We also thank Simon Buckley and the University of Bergen for their support in using LIME (www.virtualoutcrop.com/lime). Digital outcrop generation was carried out in Agisoft Photoscan. Sébastian Rohais and one anonymous reviewer are thanked for their constructive and thorough reviews. The authors have no conflict of interest to declare. The data that support the findings of this study are provided in the supplementary material or are available from the corresponding author on request.

DATA AVAILABILITY STATEMENT

The data that support the findings of this study are provided in the supplementary material or are available from the corresponding author on request.

ORCID

Timothy M. Cullen https://orcid.org/0000-0002-2497-2213
Richard E. Ll. Collier https://orcid.org/0000-0002-8001-0510
Robert L. Gawthorpe https://orcid.org/0000-0002-4352-6366
David M. Hodgson https://orcid.org/0000-0003-3711-635X
Bonita J. Barrett https://orcid.org/0000-0002-3274-822X

REFERENCES

Al Ja'Aidi, O. S. (2000). The influence of topography and flow efficiency on the deposition of turbidites. University of Leeds. PhD Thesis.

Al Ja'Aidi, O. S., McCaffrey, W. D., & Kneller, B. C. (2004). Factors influencing the deposit geometry of experimental turbidity currents: Implications for sand-body architecture in confined basins. In S. Lomas & P. Joseph (Eds.), *Geological society* (pp. 45–58). London, UK: Special Publications No. 222.

Armijo, R., Meyer, B., King, G. C. P., Rigo, A., & Papanastassiou, D. (1996). Quaternary evolution of the Corinth Rift and its implications

for the Late Cenozoic evolution of the Aegean. *Geophysical Journal International*, *126*, 11–53.

Armitage, J. J., Duller, R. A., Whittaker, A. C., & Allen, P. A. (2011). Transformation of tectonic and climatic signals from source to sedimentary archive. *Nature Geoscience*, *4*, 231–235.

Athmer, W., Groenenberg, R. M., Luthi, S. M., Donselaar, M. E., Sokoutis, D., & Willingshofer, E. (2010). Relay ramps as pathways for turbidity currents: A study combining analogue sandbox experiments and numerical flow simulations. *Sedimentology*, *57*, 806–823.

Backert, N., Ford, M. A., & Malartre, F. (2010). Architecture and sedimentology of the Kerinitis Gilbert-type fan delta, Corinth Rift, Greece. *Sedimentology*, *57*, 543–586.

Bakke, K., Kane, I. A., Martinsen, O. J., Petersen, S. A., Johansen, T. A., Hustoft, S., … Groth, A. (2013). Seismic modeling in the analysis of deep-water sandstone termination styles. *AAPG Bulletin*, *97*, 1395–1419.

Barrett, B. J., Collier, R. E. L., Hodgson, D. M., Gawthorpe, R. L., Dorrell, R., & Cullen, T. M. (2019). Quantifying faulting and base level controls on syn-rift sedimentation using stratigraphic architectures of coeval, adjacent Early-Middle Pleistocene fan deltas in Lake Corinth, Greece. *Basin Research*, 1–26. https://doi.org/10.1111/bre.12356

Barrett, B. J., Hodgson, D. M., Collier, R. E. L., & Dorrell, R. M. (2018). Novel 3D sequence stratigraphic numerical model for syn-rift basins: Analysing architectural responses to eustasy, sedimentation and tectonics. *Marine and Petroleum Geology*, *92*, 270–284.

Beckers, A., Hubert-Ferrari, A., Beck, C., Bodeux, S., Tripsanas, E., Sakellariou, D., & De Batist, M. (2015). Active faulting at the western tip of the Gulf of Corinth, Greece, from high-resolution seismic data. *Marine Geology*, *360*, 55–69.

Beckers, A., Hubert-Ferrari, A., Beck, C., Papatheodorou, G., De Batist, M., Sakellariou, D., … Demoulin, A. (2018). Characteristics and frequency of large submarine landslides at the western tip of the Gulf of Corinth. *Natural Hazards and Earth System Sciences*, *18*, 1411–1425.

Bell, R. E., McNeill, L. C., Bull, J. M., Henstock, T. J., Collier, R. E. L., & Leeder, M. R. (2009). Fault architecture, basin structure and evolution of the Gulf of Corinth rift, central Greece. *Basin Research*, *21*, 824–855.

Bilal, A., McClay, K., & Scarselli, N. (2018). Fault-scarp degradation in the central Exmouth Plateau, North West Shelf, Australia. In K. R. McClay & J. A. Hammerstein (Eds.), *Passive margins: Tectonics sedimentation and magmatism* (p. 476). London, UK: The Geological Society of London. https://doi.org/10.1144/SP476.11

Bozetti, G., Cronin, B. T., Kneller, B. C., & Mark, J. (2018). Deep-water conglomeratic megabeds: Analogues for event beds of the brae formation of the south Viking Graben, North Sea. In C. C. Turner & B. T. Cronin (Eds.), *Rift-related coarse-grained submarine fan reservoirs; The Brae Play, South Viking Graben, North Sea: AAPG Memoir* (Vol. *115*, pp. 119–154). Tulsa, Oklahoma: American Association of Petroleum Geologists.

Briole, P., Rigo, A., Lyon-Caen, H., Ruegg, J. C., Papazissi, K., Mitsakaki, C., … Deschamps, A. (2000). Active deformation of the Corinth rift, Greece: Results from repeated Global Positioning System surveys between 1990 and 1995. *Journal of Geophysical Research*, *105*, 605–625.

Burgess, P. M., & Hovius, N. (1998). Rates of delta progradation during highstands: Consequences for timing of deposition in deep-marine systems. *Journal of the Geological Society*, *155*, 217–222.

Carvajal, C. R., & Steel, R. J. (2006). Thick turbidite successions from supply-dominated shelves during sea-level highstand. *Geology*, *34*, 665–668.

Causse, C., Moretti, I., Eschard, R., & Micarelli, L. (2004). Kinematics of the Corinth Gulf inferred from calcite dating and syntectonic sedimentary characteristics. *Comptes Rendus Geoscience*, *336*(4–5), 281–290.

Collier, R. E. L., & Dart, C. J. (1991). Neogene to Quaternary rifting, sedimentation and uplift in the Corinth Basin. *Greece. Journal of the Geological Society*, *148*, 1049–1065.

Collier, R. E. L., & Gawthorpe, R. L. (1995). Neotectonics, drainage and sedimentation in central Greece: Insights into coastal reservoir geometries in syn-rift sequences. In J. J. Lambiase (Ed.), *Hydrocarbon habitat in rift basins* (Vol. *80*, pp. 165–181), London, UK: Geological Society of London.

Collier, R. E. L., Leeder, M. R., Trout, M., Ferentinos, G., Lyberis, E., & Papatheodorou, G. (2000). High sediment yields and cool, wet winters: Test of last glacial paleoclimates in the northern Mediterranean. *Geology*, *28*, 999–1002.

Cronin, B. T. (2018). Lithofabric classification and distribution of coarse-grained deep-water clastic depositional systems. In C. Turner, & B. T. Cronin (Eds.), *Rift-related coarse-grained submarine fan reservoirs; The Brae Play, South Viking Graben, North Sea: AAPG Memoir* (Vol. *115*, pp. 39–96). Tulsa, Oklahoma: American Association of Petroleum Geologists.

Dart, C. J., Collier, R. E. L., Gawthorpe, R. L., Keller, J. V. A., & Nichols, G. (1994). Sequence stratigraphy of (?)Pliocene-Quaternary synrift, Gilbert-type fan deltas, northern Peloponnesos, Greece. *Marine and Petroleum Geology*, *11*, 545–560.

Dorsey, R. J., Umhoefer, P. J., & Falk, P. D. (1997). Earthquake clustering inferred from Pliocene Gilbert-type fan deltas in the Loreto Basin, Baja California Sur, Mexico. *Geology*, *25*, 679–682.

Doutsos, T., & Piper, D. J. W. (1990). Listric faulting, sedimentation, and morphological evolution of the Quaternary eastern Corinth rift, Greece: First stages of continental rifting. *Bulletin of the Geological Society of America*, *102*, 812–829.

Doutsos, T., & Poulimenos, G. (1992). Geometry and kinematics of active faults and their seismotectonic significance in the western Corinth-Patras rift (Greece). *Journal of Structural Geology*, *14*, 689–699.

Elliott, T. (2000). Megaflute erosion surfaces and initiation of turbidite channels. *Geology*, *28*, 119–122.

Fernández-Blanco, D., de Gelder, G., Lacassin, R., & Armijo, R. (2019). Geometry of flexural uplift by continental rifting. *Tectonics*.

Flotté, N., & Sorel, D. (2001). Structural Cross Sections through the Corinth-Patras Detachment Fault-System in Northern Peleoponnesus (Aegean Arc, Greece). *Bulletin of the Geological Society of Greece*, *34*, 235–241.

Ford, M., Hemelsdaël, R., Mancini, M., & Palyvos, N. (2016). Rift migration and lateral propagation: evolution of normal faults and sediment-routing systems of the western Corinth rift (Greece). In C. Childs, R. Holdsworth, C.-A.-L. Jackson, T. Manzocchi, J. Walsh, & G. Yielding (Eds.), *The geometry and growth of normal faults* (pp. 131–168). London, UK: Geological Society of London.

Ford, M., Rohais, S., Williams, E. A., Bourlange, S., Jousselin, D., Backert, N., & Malartre, F. (2013). Tectono-sedimentary evolution

of the western Corinth rift (Central Greece). *Basin Research*, *25*, 3–25.

Ford, M., Williams, E.A., Malartre, F. & Popescu, S.-M. (2007). Stratigraphic architecture, sedimentology and structure of the Vouraikos Gilbert-type delta, Gulf of Corinth, Greece. In: G.J. Nichols, E.A. Williams & C. Paola (Eds.), *Sedimentary Processes, Environments and Basins: A Tribute to Peter Friend*, (Vol *38*, pp. 49–90). Chicester, UK: Blackwell Publishing.

Forzoni, A., Storms, J. E. A., Whittaker, A. C., & de Jager, G. (2014). Delayed delivery from the sediment factory: Modeling the impact of catchment response time to tectonics on sediment flux and fluvio-deltaic stratigraphy. *Earth Surface Processes and Landforms*, *39*, 689–704.

Fraser, S., Robinson, A., Johnson, H., Underhill, J., Kadolsky, D., Connel, R., … Ravnås, R. (2003). Upper Jurassic. In D. Evans, C. Graham, A. Armour, & P. Bathurst (Eds.), *The millennium atlas: Petroleum geologist of the central and northern North Sea* (pp. 157–189). London, UK: Geological Society of London.

Fugelli, E. M. G., & Olsen, T. R. (2007). Delineating confined slope turbidite systems offshore mid-Norway: The Cretaceous deep-marine Lysing Formation. *AAPG Bulletin*, *91*, 1577–1601. https://doi.org/10.1306/07090706137

Garland, C., Haughton, P., King, R., & Moulds, T. (1999). Capturing reservoir heterogeneity in a sand-rich submarine fan, Miller Field. In A. Fleet & S. A. Boldy (Eds.), *Petroleum geology of northwest Europe: Proceedings of the 5th conference* (pp. 1199–1208). London, UK: Geological Society of London.

Gawthorpe, R. L., Fraser, A. J., & Collier, R. E. L. (1994). Sequence stratigraphy in active extensional basins: Implications for the interpretation of ancient basin-fills. *Marine and Petroleum Geology*, *11*, 642–658.

Gawthorpe, R. L., & Leeder, M. R. (2000). Tectono-sedimentary evolution of active extensional basins. *Basin Research*, *12*, 195–218.

Gawthorpe, R. L., Leeder, M. R., Kranis, H., Skourtsos, E., Andrews, J. E., Henstra, G. A., … Stamatakis, M. (2018). Tectono-sedimentary evolution of the Plio-Pleistocene Corinth rift, Greece. *Basin Research*, *30*, 448–479. https://doi.org/10.1111/bre.12260

Ge, Z., Nemec, W., Gawthorpe, R. L., & Hansen, E. W. M. (2017). Response of unconfined turbidity current to normal-fault topography. *Sedimentology*, *64*, 932–959. https://doi.org/10.1111/sed.12333

Ge, Z., Nemec, W., Gawthorpe, R. L., Rotevatn, A., & Hansen, E. W. M. (2018). Response of unconfined turbidity current to relay-ramp topography: Insights from process-based numerical modelling. *Basin Research*, *30*, 321–343. https://doi.org/10.1111/bre.12255

Gelder, G. D., Fernández-blanco, D., Melnick, D., Duclaux, G., Bell, R. E., Jara-Muñoz, J., … Lacassin, R. (2019). Lithospheric flexure and rheology determined by climate cycle markers in the Corinth Rift. *Scientific Reports*, *9*, 1–12.

Gobo, K., Ghinassi, M., & Nemec, W. (2014). Reciprocal changes in foreset to bottomset facies in a gilbert-type delta: Response to short-term changes in base level. *Journal of Sedimentary Research*, *84*, 1079–1095.

Gobo, K., Ghinassi, M., & Nemec, W. (2015). Gilbert-type deltas recording short-term base-level changes: Delta-brink morphodynamics and related foreset facies. *Sedimentology*, *62*, 1923–1949. https://doi.org/10.1111/sed.12212

Gobo, K., Ghinassi, M., Nemec, W., & Sjursen, E. (2014). Development of an incised valley-fill at an evolving rift margin: Pleistocene eustasy and tectonics on the southern side of the Gulf of Corinth. *Greece. Sedimentology*, *61*, 1086–1119. https://doi.org/10.1111/sed.12089

Goldsworthy, M., & Jackson, J. (2001). Migration of activity within normal fault systems: Examples from the quaternary of mainland Greece. *Journal of Structural Geology*, *23*, 489–506.

Gupta, S., Underhill, J. R., Sharp, I. R., & Gawthorpe, R. K. (1999). Role of fault interactions in controlling synrift sediment dispersal patterns: Miocene, Abu Alaqa Group, Suez Rift, Sinai, Egypt. *Basin Research*, *11*, 167–189. https://doi.org/10.1046/j.1365-2117.1999.00300.x

Harms, J. C., Southard, J. B., Spearing, D. R., & Walker, R. G. (1975). Depositional environments as interpreted from primary sedimentary and stratigraphic sequences. In: Depositional Environments as Interpreted from Primary Sedimentary and Stratigraphic Sequences. SEPM Short course 2.

Haughton, P., Davis, C., McCaffrey, W., & Barker, S. (2009). Hybrid sediment gravity flow deposits - Classification, origin and significance. *Marine and Petroleum Geology*, *26*, 1900–1918.

Hemelsdaël, R., & Ford, M. (2016). Relay zone evolution: A history of repeated fault propagation and linkage, central Corinth rift, Greece. *Basin Research*, *28*, 34–56. https://doi.org/10.1111/bre.12101

Henstra, G. A., Grundvåg, S. A., Johannessen, E. P., Kristensen, T. B., Midtkandal, I., Nystuen, J. P., … Windelstad, J. (2016). Depositional processes and stratigraphic architecture within a coarse-grained rift-margin turbidite system: The Wollaston Forland Group, east Greenland. *Marine and Petroleum Geology*, *76*, 187–209.

Hodgson, D. M., & Haughton, P. D. W. (2004). Impact of syndepositional faulting on gravity current behaviour and deep-water stratigraphy: Tabernas-Sorbas Basin, SE Spain. In S. Lomas & P. Joseph (Eds.), *Confined turbidite systems* (pp. 135–158). London, UK: Geological Society of London.

Hodgson, D. M., Kane, I. A., Flint, S. S., Brunt, R. L., & Ortiz-Karpf, A. (2016). Time-transgressive confinement on the slope and the progradation of basin-floor fans: Implications for the sequence stratigraphy of deep-water deposits. *Journal of Sedimentary Research*, *86*, 73–86. https://doi.org/10.2110/jsr.2016.3

Hoyal, D., Van Wagoner, J. C., Adair, N., Deffenbaugh, M., Li, D., Sun, T., …Giffin, D. (2003). Sedimentation from jets: A depositional model for clastic deposits of all scales and environments. AAPG Annual Conference & Exhibition extended abstract.

Jackson, C.-A.-L., Kane, K., Larsen, E., Evrard, E., Elliott, G., & Gawthorpe, R. (2012). Variability in syn-rift structural style associated with a mobile substrate and implications for trap definition and reservoir distribution in extensional basins: A subsurface case study from the south Viking Graben, Offshore Norway. *AAPG Search & Discovery*, *10423*, 1–7.

Jerolmack, D. J., & Paola, C. (2010). Shredding of environmental signals by sediment transport. *Geophysical Research Letters*, *37*, 1–5.

Jones, M. A., Cronin, B. T., & Allerton, S. (2018). A depositional model for the T-block Thelma field, UKCS block 16/17. In C. C. Turner & B. T. Cronin (Eds.), *Rift-related coarse-grained submarine fan reservoirs; The Brae Play, South Viking Graben, North Sea: AAPG Memoir* (Vol. *115*, pp. 307–338). Tulsa, Oklahoma: American Association of Petroleum Geologists.

Kane, I. A., Catterall, V., McCaffrey, W. D., & Martinsen, O. J. (2010). Submarine channel response to intrabasinal tectonics: The influence of lateral tilt. *AAPG Bulletin*, *94*, 189–219. https://doi.org/10.1306/08180909059

Kane, I. A., Dykstra, M. L., Kneller, B. C., Tremblay, S., & McCaffrey, W. D. (2009). Architecture of a coarse-grained channel-levée system: The Rosario Formation, Baja California, Mexico. *Sedimentology*, *56*, 2207–2234.

Kane, I. A., Pontén, A. S. M., Vangdal, B., Eggenhuisen, J. T., & Hodgson, D. M. (2017). The stratigraphic record and processes of turbidity current transformation across deep-marine lobes. *Sedimentology*, *64*, 1236–1273.

Kostaschuk, R. A., & McCann, S. B. (1989). Submarine slope stability of a fjord delta: Bella Coola. *British Columbia. Géographie Physique Et Quaternaire*, *43*, 87. https://doi.org/10.7202/032756ar

Koutsouveli, A., Mettos, A., Tsapralis, V., Tsala-Monopoli, S., & Iokim, C. (1989). *Geological map of Greece: 1:50,000, Xylokastro Sheet*. Athens, Greece: IGME Publications.

Leeder, M. R., Mark, D. F., Gawthorpe, R. L., Kranis, H., Loveless, S., Pedentchouk, N., … Stamatakis, M. (2012). A 'Great Deepening': Chronology of rift climax, Corinth rift, Greece. *Geology*, *40*, 999–1002. https://doi.org/10.1130/G33360.1

Leppard, C. W., & Gawthorpe, R. L. (2006). Sedimentology of rift climax deep water systems; Lower Rudeis Formation, Hammam Faraun Fault Block, Suez Rift, Egypt. *Sedimentary Geology*, *191*, 67–87.

Lewis, M. M., Jackson, C. A. L., & Gawthorpe, R. L. (2015). Tectono-sedimentary development of early syn-rift deposits: The Abura Graben, Suez Rift, Egypt. *Basin Research*, *29*, 327–351.

Lowe, D. R. (1982). Sediment gravity flows: II Depositional models with special reference to the deposits of high-density turbidity currents. *Journal of Sedimentary Petrology*, *52*, 279–297. https://doi.org/10.1306/212F7F31-2B24-11D7-8648000102C1865D

MacDonald, H. A., Peakall, J., Wignall, P. B., & Best, J. (2011). Sedimentation in deep-sea lobe-elements: Implications for the origin of thickening-upward sequences. *Journal of the Geological Society London*, *168*, 319–331.

McArthur, A. D., Hartley, A. J., Archer, S. G., Jolley, D. W., & Lawrence, H. M. (2016). Spatiotemporal relationships of deep-marine, axial, and transverse depositional systems from the synrift Upper Jurassic of the central North Sea. *AAPG Bulletin*, *100*, 1469–1500. https://doi.org/10.1306/04041615125

McLeod, A. E., Underhill, J. R., Davies, S. J., & Dawers, N. H. (2002). The influence of fault array evolution on synrift sedimentation patterns: Controls on deposition in the strathspey-brent-statfjord half graben, northern North Sea. *AAPG Bulletin*, *86*, 1061–1093.

McNeill, L. C., Cotterill, C. J., Bull, J. M., Henstock, T. J., Bell, R., & Stefatos, A. (2007). Geometry and slip rate of the Aigion fault, a young normal fault system in the western Gulf of Corinth. *Geology*, *35*, 355–358. https://doi.org/10.1130/G23281A.1

McNeill, L. C., Cotterill, C. J., Henstock, T. J., Bull, J. M., Stefatos, T. J., Collier, R. E. L., … Hicks, S. E. (2005). Active faulting within the offshore western Gulf of Corinth, Greece: Implications for models of continental rift deformation. *Geology*, *33*, 241–244. https://doi.org/10.1130/G21127.1

Mcneill, L. C., Shillington, D. J., Carter, G. D. O., Everest, J. D., Gawthorpe, R. L., Miller, C., … Ford, M. (2019). High-resolution record reveals climate-driven environmental and sedimentary changes in an active rift. *Scientific Reports*, *9*, 1–11.

Nixon, C. W., McNeill, L. C., Bull, J. M., Bell, R. E., Gawthorpe, R. L., Henstock, T. J., … Kranis, H. (2016). Rapid spatiotemporal variations in rift structure during development of the Corinth Rift, central Greece. *Tectonics*, *35*, 1225–1248.

Papanikolaou, D. J., & Royden, L. H. (2007). Disruption of the Hellenic arc: Late Miocene extensional detachment faults and steep Pliocene-Quaternary normal faults — Or what happened at Corinth ? *Tectonics*, *26*, 1–16.

Pirazzoli, P. A., Stiros, S. C., Fontugne, M., & Arnold, M. (2004). Holocene and Quaternary uplift in the central part of the southern coast of the Corinth Gulf (Greece). *Marine Geology*, *212*, 35–44.

Postma, G. (1986). Classification for sediment gravity-flow deposits based on flow conditions during sedimentation. *Geology*, *14*, 291–294.

Postma, G., & Cruickshank, C. (1988). Sedimentology of a late Weichselian to Holocene terraced fan delta, Varangerfjord, Northern Norway. In W. Nemec & R. J. Steel (Eds.), *Fan deltas: Sedimentology and tectonic settings* (pp. 144–157). London, UK: Blackie & Son.

Prior, D. B., & Bornhold, B. (1988). Submarine morphology and processes of fjord fan deltas and related high-gradient systems: modern examples from British Columbia. In W. Nemec, & R. J. Steel (Eds.), *Fan deltas: Sedimentology and tectonic settings* (pp. 125–143). London, UK: Blackie & Son.

Prior, D. B., Wiseman, W. J., & Bryant, W. R. (1981). Submarine chutes on the slopes of fjord deltas. *Nature*, *290*, 326–328.

Prosser, S. (1993). Rift-related linked depositional systems and their seismic expression. *Geological Society of London Special Publication*, *71*, 35–66.

Ravnås, R., & Steel, R. J. (1997). Contrasting styles of Late Jurassic syn-rift turbidite sedimentation: A comparative study of the Magnus and Oseberg areas, northern North Sea. *Marine and Petroleum Geology*, *14*, 417–449.

Ravnås, R., & Steel, R. J. (1998). Architecture of marine rift basin successions. *AAPG Bulletin*, *82*, 110–146.

Reading, H. G., & Richards, M. (1994). Turbidite systems in deep-water basin margins classified by grain size and feeder system. *AAPG Bulletin*, *78*, 792–822.

Rohais, S., Eschard, R., Ford, M., Guillocheau, F., & Moretti, I. (2007). Stratigraphic architecture of the Plio-Pleistocene infill of the Corinth Rift: Implications for its structural evolution. *Tectonophysics*, *440*, 5–28. https://doi.org/10.1016/j.tecto.2006.11.006

Rohais, S., Eschard, R., & Guillocheau, F. (2008). Depositional model and stratigraphic architecture of rift climax Gilbert-type fan deltas (Gulf of Corinth, Greece). *Sedimentary Geology*, *210*, 132–145.

Rohais, S., Joannin, S., Colin, J. P., Suc, J. P., Guillocheau, F., & Eschard, R. (2007). Age and environmental evolution of the syn-rift fill of the southern coast of the Gulf of Corinth (Akrata-Derveni region, Greece). *Bulletin De La Societe Geologique De France*, *178*, 231–243.

Rohais, S., & Moretti, I. (2017). Structural and stratigraphic architecture of the Corinth Rift (Greece): An integrated onshore to offshore basin-scale synthesis. In F. Roure, A. A. Amin, S. Khomsi, & M. A. Al Garni (Eds.), *Lithosphere dynamics and sedimentary basins of the Arabian plate and surrounding areas* (pp. 89–120). Switzerland: Springer International Publishing, Frontiers in Earth Sciences.

Rubi, R., Rohais, S., Bourquin, S., Moretti, I., & Desaubliaux, G. (2018). Processes and typology in Gilbert-type delta bottomset deposits based on outcrop examples in the Corinth Rift. *Marine and Petroleum Geology*, *92*, 193–212. https://doi.org/10.1016/j.marpetgeo.2018.02.014

Scholz, C. A., Moore, T. C., Hutchinson, D. R., Golmshtok, A. J., Klitgord, K. D., & Kurotchkin, A. G. (1998). Comparative sequence stratigraphy of low-latitude versus high-latitude lacustrine rift basins: Seismic data examples from the East African and Baikal rifts. *Palaeogeography, Palaeoclimatology, Palaeoecology*, *140*, 401–420.

Scholz, C. A., Rosendahl, B. R., & Scott, D. L. (1990). Development of coarse grained-facies in lacustrine rift basins: Example from East Africa. *Geology*, *18*, 140–144.

Sharp, I. R., Gawthorpe, R. L., Underhill, J. R., & Gupta, S. (2000). Fault-propagation folding in extensional settings: Examples of structural style and synrift sedimentary response from the Suez rift, Sinai, Egypt. *Bulletin of the Geological Society of America*, *112*, 1877–1899.

Skourtsos, E., & Kranis, H. (2009). Structure and evolution of the western Corinth Rift, through new field data from the Northern Peloponnesus. In U. Ring & B. Wernicke (Eds.), *Extending a continent: Architecture, rheology and heat budget* (Vol. *321*, pp. 119–138). London, UK: Geological Society of London.

Skourtsos, E., Kranis, H., Zambetakis-Lekkas, A., Gawthorpe, R., & Leeder, M. (2016). Alpine basement outcrops at northern peloponnesus: Implications for the early stages in the evolution of the Corinth Rift. *Bulletin of the Geological Society of Greece*, *50*, 153–163.

Soreghan, M. J., Scholz, C. A., & Wells, J. T. (1999). Coarse-grained, deep-water sedimentation along a border fault margin of Lake Malawi, Africa: Seismic stratigraphic analysis. *Journal of Sedimentary Research*, *69*, 832–846.

Stevenson, C. J., Jackson, C.-L., Hodgson, D. M., Hubbard, S. M., & Eggenhuisen, J. T. (2015). Deep-water sediment bypass. *Journal of Sedimentary Research*, *85*, 1058–1081. https://doi.org/10.2110/jsr.2015.63

Strachan, L. J., Rarity, F., Gawthorpe, R. L., Wilson, P., Sharp, I., & Hodgetts, D. (2013). Submarine slope processes in rift-margin basins, Miocene Suez Rift, Egypt. *Bulletin of the Geological Society of America*, *125*, 109–127.

Sumner, E. J., Talling, P. J., & Amy, L. A. (2009). Deposits of flows transitional between turbidity current and debris flow. *Geology*, *37*, 991–994.

Taylor, B., Weiss, J. R., Goodliffe, A. M., Sachpazi, M., Laigle, M., & Hirn, A. (2011). The structures, stratigraphy and evolution of the Gulf of Corinth rift, Greece. *Geophysical Journal International*, *185*, 1189–1219.

Trout, M. N. (1999). Sediment transport and deposition across active faulted rift margins. PhD Thesis, University of Leeds.

Tsoflias, P., Fleury, J., & Iokim, C. (1993). *Geological map of Greece: 1:50,000, Derveni sheet*. Athens, Greece: IGME Publications.

Turner, C., & Allen, P. A. (1991). The Central Brae Field, block 16/7a, UK North Sea. In I. Abbotts (Ed.), *United Kingdom Oil and Gas Fields; 25 years Commemorative Volume, Geological Society Memoir* (Vol. *14*, pp. 49–54). London, UK: Geological Society of London.

Turner, C. C., Bastidas, R. E., Connell, E. R., & Petrik, F. E. (2018). Proximal submarine fan reservoir architecture and development in the upper Jurassic brae formation of the brae fields, south Viking Graben, U.K. North Sea. In C. C. Turner & B. T. Cronin (Eds.) *Rift-related coarse-grained submarine fan reservoirs; The Brae Play, South Viking Graben, North Sea: AAPG Memoir* (Vol. *115*, pp. 213–256). Tulsa, Oklahoma: American Association of Petroleum Geologists.

Turner, C. C., Cronin, B. T., Cronin, B. T., Riley, L. A., Patruno, S., Reid, W. T. L. R., … Jackson, C. A. (2018). The south Viking graben: Overview of upper Jurassic rift geometry, biostratigraphy, and extent of brae play submarine fan systems. In C. C. Turner & B. T. Cronin (Eds.), *Rift-related coarse-grained submarine fan reservoirs; The Brae Play, South Viking Graben, North Sea: AAPG Memoir* (Vol. *115*, pp. 9–38). Tulsa, Oklahoma: American Association of Petroleum Geologists.

Westaway, R. (2002). The Quarternary evolution of the Gulf of Corinth, central Greece: Coupling between surface processes and flow in the lower continental crust. *Tectonophysics*, *348*, 269–318.

Young, M. J., Gawthorpe, R. L., & Sharp, I. R. (2002). Architecture and evolution of syn-rift clastic depositional systems towards the tip of a major fault segment, Suez rift. *Egypt. Basin Research.*, *14*, 1–23. https://doi.org/10.1046/j.1365-2117.2002.00162.x

Zhang, J., Burgess, P. M., Granjeon, D., & Steel, R. (2019). Can sediment supply variations create sequences? Insights from stratigraphic forward modelling. *Basin Research*, *31*, 274–289.

Zhang, J., Kim, W., Olariu, C., & Steel, R. (2019). Accommodation-versus supply-dominated systems for sediment partitioning to deep water. *Geology*, *47*, 1–4. https://doi.org/10.1130/G45730.1

Zhong, X., Escalona, A., Sverdrup, E., & Bukta, K. E. (2018). Impact of fault evolution in Gilbert-type fan deltas in the Evrostini area, south-central Gulf of Corinth, Greece. *Marine and Petroleum Geology*, *95*, 82–99.

Zitter, T. A. C., Grall, C., Henry, P., Özeren, M. S., Çağatay, M. N., Şengör, A. M. C., … Géli, L. (2012). Distribution, morphology and triggers of submarine mass wasting in the Sea of Marmara. *Marine Geology*, *329–331*, 58–74.

SUPPORTING INFORMATION

Additional supporting information may be found online in the Supporting Information section.

How to cite this article: Cullen TM, Collier REL, Gawthorpe RL, Hodgson DM, Barrett BJ. Axial and transverse deep-water sediment supply to syn-rift fault terraces: Insights from the West Xylokastro Fault Block, Gulf of Corinth, Greece. *Basin Res*. 2019;00:1–35. https://doi.org/10.1111/bre.12416